



Check for updates

Cite this: *Inorg. Chem. Front.*, 2020, 7, 2396

## Cyclometalated Ir(III) complexes towards blue-emissive dopant for organic light-emitting diodes: fundamentals of photophysics and designing strategies

Sunhee Lee and Won-Sik Han \*

The main difficulties hindering development of a deep-blue phosphorescent cyclometalated Ir(III) complex are insufficient colour purity, *i.e.*, failure to achieve ideal Commission Internationale de L'Eclairage (CIE) coordinates of (0.14, 0.09), and insufficient emission efficiency and stability. The latter problem is due to the highly energetic and hot excited states of these complexes, which yield faster decomposition. Therefore, control of the excited-state properties of cyclometalated Ir(III) complexes through systematic chemical modification of the ligands is being extensively investigated, with the aim of developing efficient and stable blue phosphorescent materials. The most common strategies towards achievement of a blue phosphorescent cyclometalated Ir(III) complex involve (1) substitution of electron-withdrawing F atoms at the cyclometalating ligands that stabilise the HOMO orbitals and (2) use of a heteroleptic system with electron-rich ancillary ligands bearing a 5-membered ring heterocycle to increase the LUMO energy level. However, the C–F bonds on the cyclometalating ligands have been found to be inherently unstable during device operation; thus, other types of electron-withdrawing groups (*e.g.*, the cyano, trifluoromethyl, and sulfonyl groups) have been applied. Along with phosphorescence colour tuning to blue, the influence of the ligand structure on the photoluminescence quantum yield (PLQY) is also being intensively investigated. Two major PLQY lowering mechanisms for blue emissive Ir(III) complexes have been identified: (1) the vibronic-coupled non-radiative decay process and (2) crossing from the emissive state to an upper non-emissive  $^3\text{MC}$  excited state. To enhance the PLQY, mechanism (1) can be suppressed by employing rigid ligand frameworks to restrict intramolecular motion, whereas mechanism (2) can be prevented by destabilising the  $^3\text{MC}$  state using strong  $\sigma$  donor ligands such as N-heterocyclic carbenes. This review summarises the fundamental photophysics of cyclometalated Ir(III) complexes and surveys design strategies for efficient blue phosphorescent Ir(III) complexes, to provide a guide for future research in this field.

Received 2nd January 2020,

Accepted 28th April 2020

DOI: 10.1039/d0qi00001a

rsc.li/frontiers-inorganic

### 1. Introduction

Organic light-emitting diodes (OLEDs) have attracted considerable interest in the display field in recent decades because of their various advantages, such as their light weight, high contrast ratio, wide viewing angle, improved energy efficiency, and excellent design versatility. The OLED working principle involves operation using two kinds of radiative relaxation process, *i.e.*, fluorescence and phosphorescence, which originate from singlet and triplet excited states, respectively. In theory, utilisation of triplet excitons along with singlet excitons

yields 100% efficiency;<sup>1,2</sup> therefore, intensive research has been performed on materials that can achieve high triplet excited states with high photoluminescence quantum yield (PLQY). It is well-known that the triplet excited state can be generated efficiently *via* heavy-atom-induced spin-orbit coupling. Among the transition metal complexes, cyclometalated Ir(III) complexes have been deemed the most efficient because of their highly efficient populations of triplet excited states, which induce radiative decay processes.<sup>3</sup> Indeed, almost 100% internal quantum efficiency for conversion of electric energy to photons has been achieved.<sup>2,4–12</sup>

In this regard, cyclometalated Ir(III) complexes play an essential role in OLED applications such as flat panel displays and solid-state lighting.<sup>1,13–15</sup> Previous studies have established the structure–property relationships within cyclometalated Ir(III) complexes that enable high-efficiency phosphor-

Department of Chemistry, Seoul Women's University, 621 Hwarang-ro, Seoul 01797, Republic of Korea. E-mail: wshan@swu.ac.kr

escence emission with full spectral coverage spanning the near ultraviolet (UV) to near infrared. However, phosphorescence tuning over the entire visible spectrum remains a challenge. The design and synthesis of deep-blue-emitting cyclometalated Ir(III) complexes is particularly difficult. Although high external quantum efficiencies (EQEs) exceeding 30% have been achieved for green and red OLED devices,<sup>16–20</sup> high EQEs for deep-blue OLED devices have rarely been reported.<sup>21–24</sup>

The main difficulties in developing deep-blue-emissive Ir(III) complexes are the following: (1) they lack sufficient colour purity for the ideal Commission Internationale de L'Eclairage (CIE) coordinates of (0.14, 0.09), (2) they have insufficient emission efficiency, and (3) attainment of an appropriate host and carrier transport materials with sufficient triplet energy levels is challenging. (Note: The materials for the host and carrier transport materials are not discussed in this review.) These difficulties are due to the highly energetic excited states of blue phosphors, which can yield faster decomposition than those of green and red phosphors.<sup>25–28</sup> In addition, the upper-lying excited states of blue-emissive Ir(III) complexes can induce several degradation processes, for example, triplet-triplet annihilation,<sup>29,30</sup> triplet-polaron annihilation,<sup>31</sup> and polaron-polaron annihilation.<sup>32</sup>

Note that review articles of blue phosphorescent cyclometalated Ir(III) complexes for applications in OLEDs have been well presented previously.<sup>33–50</sup> In this review, we will discuss the current research status regarding development of cyclometalated Ir(III) complexes towards a blue-emissive dopant for OLEDs. We summarise the fundamental photophysics of cyclometalated Ir(III) complexes, considering radiative and non-radiative (NR) decay processes (section 2). We then discuss the structure–property relationship dependence on the ancillary ligand (section 3). We hope this review will be helpful to OLED researchers working to design efficient deep-blue phosphorescent Ir(III) complexes.

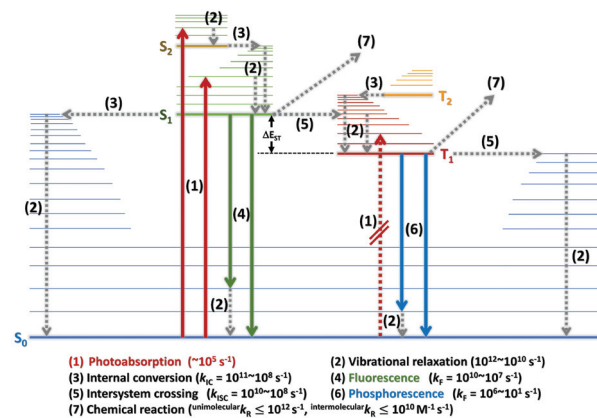


Fig. 1 Modified Jablonski diagram with time scales for photophysical processes in molecular system. Bold and dotted lines indicate radiative and non-radiative (NR) decay processes, respectively.

## 2. Fundamental photophysics of cyclometalated Ir(III) complexes

### 2.1. General molecular photophysics upon excitation

When a molecule absorbs energy (e.g., photons), the electrons in the ground state become excited and decays along multiple photophysical pathways. These processes can be presented schematically as an energy diagram known as a 'Jablonski diagram',<sup>51</sup> as depicted in Fig. 1. The main processes can be classified as photoabsorption, vibrational relaxation, internal conversion (IC), fluorescence, intersystem crossing (ISC), phosphorescence, and photochemical processes, and summarised as follows.

(1) Photoabsorption: As a molecule absorbs photons, an electron is excited from the singlet ground state ( $S_0$ ), to the



Sunhee Lee

*Sunhee Lee obtained her B.Sc. degree in 2017 from Seoul Women's University, and she also received her M.Sc. degree from the same university in 2019. She is currently a Ph.D. student under the supervision of Prof. Won-Sik Han in Seoul Women's University. She works on the design and synthesis of the transition-metal complex for organic light-emitting diodes and photocatalysts for organic synthesis.*



Won-Sik Han

*Won-Sik Han was born in Seoul, South Korea. He obtained his B.Sc. (2004) and Ph.D. (2011) degrees from Korea University. During Ph.D., he worked on the synthesis of organic and organometallic materials for OLED applications under the supervision of Prof. Sang Ook Kang. He spends two years as a post-doc at Northwestern University worked on solar fuels via artificial photosynthesis under the supervision of Prof. Michael R. Wasielewski. After that, he came back to South Korea and joined the faculty of Seoul Women's University. His main research interests are the synthesis of organic electronic materials and photocatalysts for organic synthesis.*

lowest ( $S_1$ ) or higher singlet excited states ( $S_n$ ). The transition rate is very fast, at  $>10^{15} \text{ s}^{-1}$ . In general, a transition from  $S_0$  to the lowest triplet state ( $T_1$ ) has low probability because the electron spin is parallel to the ground-state spin; thus, this transition is called 'forbidden'. However, this forbidden transition can be observed under specific conditions, for example, for internal and external heavy-atom effects with very low extinction coefficients ( $\epsilon$ ), with for which  $\epsilon_{\text{max}} = 10^{-1}\text{--}10^{-2}$ .

(2) Vibrational relaxation: Immediately after excitation to  $S_1$  or  $S_n$ , the molecule population distribution in the Franck-Condon state of the higher excited-vibrational states ( $v' \geq 1$ ) relaxes to a less energetic vibrational state ( $v' = 0$ ) through vibrational energy transfer. This process also occurs immediately after IC and intersystem crossing. The vibrational relaxation rate is in the range of a few picoseconds, at  $>10^{12} \text{ s}^{-1}$ .

(3) IC: This process involves a change in the electronic states, for example,  $S_n$  to  $S_{n-1}$ , which have energetically degenerate vibrational states. Therefore, there is no energy change and this process is radiationless. The IC range is  $<10^8 \text{ s}^{-1}$  and depends on the energy gap between the  $S_n$  and  $S_{n-1}$  states according to the 'Energy Gap Law'.

(4) Fluorescence: This process is a radiative transition from  $S_1$  to  $S_0$ , as allowed by the selection rules, at a rate of  $\leq 10^9 \text{ s}^{-1}$ . As the IC rate from  $S_n$  to  $S_{n-1}$  is very high (in the picoseconds range), most fluorescence occurs from the lowest  $S_1$  state; this is called 'Kasha's Rule'.

(5) ISC: This process is similar to IC. However, although the molecular spin state remains the same for IC, the ISC process requires a change in spin state. The latter process involves transitions from  $S_1$  to the higher excited-vibrational states of  $T_1$  and  $T_n$ , followed by relaxation to less energetic vibrational states (similar to IC). The ISC rate is in the range of  $10^{12} \text{ s}^{-1}$  and depends on the degree of spin-orbit coupling and the 'El-Sayed Rule'. The transition from  $T_1$  to  $S_0$  is also an ISC process, but with a lower transition rate ( $\leq 10^6 \text{ s}^{-1}$ ) than the  $S_1 \rightarrow T_1$  transition according to the "Energy Gap Law" (the energy gap between the  $T_1$  and  $S_0$  states is usually larger than that between the  $S_1$  and  $T_1$  states).

(6) Phosphorescence: This process is another radiative transition and involves transition from the  $T_1$  to  $S_0$  states. As the direct formation of  $T_1$  from  $S_0$  is a forbidden transition, the  $T_1$  state is usually generated *via* the following sequence: excitation from  $S_0$  to  $S_n \rightarrow$  rapid IC from  $S_n$  to  $S_1 \rightarrow$  ISC from  $S_1$  to  $T_1$ . The phosphorescence rate for organic compounds is approximately  $10^3 \text{ s}^{-1}$  but is much higher for organometallic complexes that possess heavy metals, being in the range of  $>10^6 \text{ s}^{-1}$ .

(7) Photochemical processes: The energy or electron in the excited state can participate in chemical reactions. In general, these processes occur from the  $S_1$  and  $T_1$  states. In the case of the unimolecular reaction process, the reaction rate is in the range of  $\leq 10^{12} \text{ s}^{-1}$ . For the intermolecular (bimolecular) reaction process, the reaction rate depends on the solvent temperature ( $T$ ) and viscosity ( $\leq 10^{10} \text{ M}^{-1} \text{ s}^{-1}$ ).

In particular, triplet-related processes are a major focus in the context of cyclometalated Ir(III) complexes for OLED appli-

cation, as the maximum internal quantum efficiency for conversion of electric energy to photons can be achieved through phosphorescence.

## 2.2. General photophysics in the cyclometalated Ir(III) complex

**2.2.1. Transitions from ground to excited states.** It is generally accepted that photoexcitation induces transitions from  $S_0$  to the singlet ligand centred state ( $^1\text{LC}$ ) and singlet metal-to-ligand charge transfer ( $^1\text{MLCT}$ ) state. In addition, triplet MLCT ( $^3\text{MLCT}$ ) and LC ( $^3\text{LC}$ ) transitions occur *via* Ir-induced strong spin-orbit coupling (SOC), yielding four electronic states:  $^1\text{LC}$ ,  $^1\text{MLCT}$ ,  $^3\text{MLCT}$ , and  $^3\text{LC}$ .

As an example, Fig. 2 shows the absorption spectrum of the well-known cyclometalated homoleptic Ir(III) complex, *fac*-tris [2-phenylpyridine]iridium(III), *fac*-Ir(ppy)<sub>3</sub>, (1). The absorption spectrum involves strong  $^1\text{LC}$  spin-allowed  $\pi\text{--}\pi^*$  transitions at  $<300 \text{ nm}$  and spin-allowed d– $\pi^*$  transitions ( $^1\text{MLCT}$ ) in the 320–430 nm range. The  $>435 \text{ nm}$  absorptions are attributable to a spin-forbidden  $^3\text{MLCT}$  transition with very low  $\epsilon$ ; this is a consequence of the heavy-atom effect yielding a strong SOC.<sup>52</sup> However, it should be noted that the lowest energy state of **1** is a hybrid state with  $^3\text{MLCT}$  and  $^3\text{LC}$  characteristics (*vide infra*).

These assignments for the transitions of **1** are supported by theoretical calculations.<sup>53–55</sup> According to those calculations, the molecular orbitals mainly participating in generation of the lowest triplet state are from the highest occupied molecular orbital (HOMO) to the lowest unoccupied molecular orbital (LUMO). As shown in Fig. 2b, the HOMO is delocalised over the Ir  $t_{2g}$  orbital and the  $\pi$  orbitals of the phenyl ring in the 2-ppy ligand, whereas the LUMO exclusively involves the  $\pi^*$  orbitals of the pyridine ring in the 2-ppy. Therefore, one of the causes of the  $S_0 \rightarrow T_1$  transition is charge transfer from the 5d Ir metal orbital to the ppy ligands. Further studies involving time-dependent density functional theory (TD-DFT) calculations have indicated that the lowest triplet state is in a hybrid form of the MLCT and LC transition states.<sup>56,57</sup> In the triplet manifold, the dominant LC state may be lowest. This is because the singlet–triplet splitting from the electron-exchange interaction is much smaller for MLCT than LC  $\pi\text{--}\pi^*$ ,

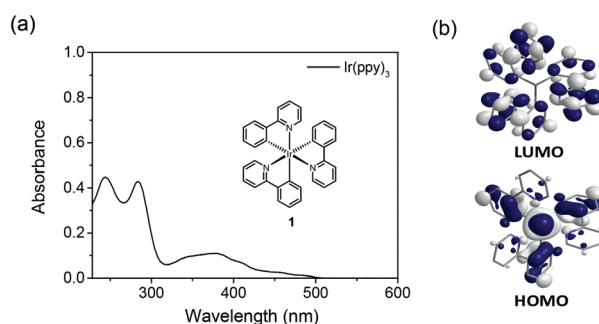


Fig. 2 (a) Absorption spectrum in  $10 \mu\text{M}$  solution of dichloromethane (inset: chemical structure) and (b) orbital contributions of HOMO and LUMO of **1**.

as the orbitals in the MLCT excited state have greater spatial extension. The optimised structure of the lowest triplet energy state indicates broken  $C_3$  symmetry and excitation localised on a single ligand, supporting hybridisation in the triplet excited states. More detailed analysis based on multi-configuration self-consistent field orbitals and second-order configurational interactions have been performed to study the different radiative and NR processes of *fac*-**1** and *mer*-**1**.<sup>58</sup> Heteroleptic<sup>59,60</sup> and bis-tridentate<sup>61</sup> Ir(III) complexes have also yielded similar calculation results.

**2.2.2. Radiative decay processes from triplet state.** As mentioned above, photoexcitation generates the LC and MLCT transition states. IC occurs from the higher  $^1\text{LC}$  state to the lower  $^1\text{MLCT}$  state with a time constant exceeding 100 fs.<sup>62</sup> Subsequently, the  $^1\text{MLCT}$  state undergoes ultrafast (<100 fs) ISC to the  $^3\text{MLCT}$  state as a result of the Ir-induced strong SOC, followed by vibrational relaxation to the respective lowest-lying vibrational state in less than 700 fs.<sup>63–67</sup>

Yersin *et al.* investigated the detailed properties of the emitting triplet state of **1**, including the corresponding radiative and NR transitions.<sup>52,66</sup> The lowest triplet state can be divided into three substates: **I**, **II**, and **III**. For most organometallic complexes containing transition metal ions, the transition between the lowest substate **I** and  $S_0$  is forbidden, but the other transitions from **II** and **III** to  $S_0$  are permitted.<sup>68–71</sup> The same results were found for **1**.<sup>66</sup> Indeed, three emissive triplet substates, **I–III**, of **1** in tetrahydrofuran (THF) solution were identified from the temperature-dependent emission spectra (1.2 K  $\leq T \leq$  300 K) and classified as substates of a  $^3\text{MLCT}$  state. Through further combined analysis with application of high magnetic fields, the energy differences between the substates were successfully estimated, *i.e.*,  $\Delta E_{\text{II–I}} = 13.5 \text{ cm}^{-1}$  and  $\Delta E_{\text{III–I}} = 83.5 \text{ cm}^{-1}$ , as depicted in Fig. 3. This relatively large total zero-field splitting (ZFS) indicates that the lowest triplet state of **1** is a  $^3\text{MLCT}$  state. The same assignments were concluded from theoretical calculations.<sup>53,56,72</sup>

Heteroleptic Ir(III) complexes possess more complex photochemical processes than those of a homoleptic system, because the presence of the ancillary ligand ( $L'$ ) induces additional

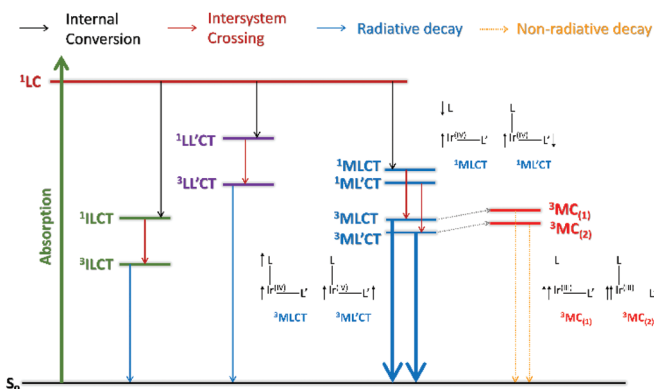


Fig. 4 Main decay processes from excited state of heteroleptic Ir(III) complex system.

transitions such as L'C and ML'CT. This is in addition to the ligand-to-ligand charge transfer (LL'CT) transition that occurs between a main ligand and ancillary ligand, as shown in Fig. 4.

The most well-known blue-emissive heteroleptic Ir(III) is likely a bis[2-(4,6-difluorophenyl)pyridinato- $C^2,N$ ](picolinato) iridium(III), commonly known as FIripic (2).<sup>73</sup> Fig. 5 shows typical emission spectra of 2 at RT and 77 K. The RT emission spectrum exhibits blue phosphorescence peaks at 471 and 495 nm with fine vibronic structure, which are virtually independent of the solvent polarity. These observations indicate that the emitting lowest triplet state has a predominantly  $^3\text{LC}$  character with a minor  $^3\text{MLCT}$  contribution. Thus, if the cyclometalated Ir(III) complex emission has a non-vibronic structure and the emission changes depending on the solvent polarity, the lowest triplet state has a predominantly  $^3\text{MLCT}$  character. At low temperature (77 K), the emission spectrum of 2 shows narrower and highly structured emission bands at 461 and 495 nm, indicating that the  $^3\text{LC}$  character is increased at this temperature. A small thermally induced Stokes shift ( $\Delta E_S$ ) with of 10 nm also indicates that the nature of the lowest triplet state in 2 is based on the  $^3\text{LC}$  state. In general, small and large  $\Delta E_S$  indicate  $^3\text{LC}$  and  $^3\text{MLCT}$  excited states, respectively.<sup>74–76</sup> The PLQY of 2 in dilute solution was initially reported to be approximately 0.6. Note, however, that this value was later corrected to higher values of >0.90.<sup>77–79</sup> Accordingly, the radiative- and NR constants of 2 were estimated to be  $k_r = 5 \times 10^5 \text{ s}^{-1}$  and  $k_{\text{nr}} = 0.5 \times 10^5 \text{ s}^{-1}$ , respectively.

**2.2.3. Non-radiative (NR) decay processes from triplet state.** After the  $T_1$  state is generated, not only the radiative decay process with rate of  $k_r$ , but also multiple NR processes with rates of  $k_{\text{nr}}$ , can appear; these processes then compete with each other. Depending on the presence of a temperature effect, these decay processes can be divided into two types: temperature-independent and -dependent.

Temperature-independent decay processes occur *via* direct crossing between the two potential energy surfaces of the triplet and ground states. These are vibronic-coupled NR decay process, as studied in detail by Samuel *et al.*<sup>80,81</sup> Those

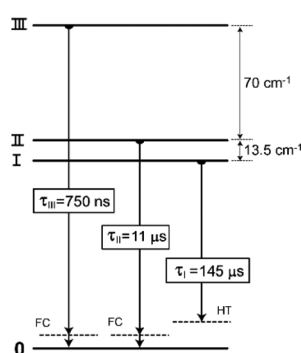


Fig. 3 Energy levels for three lowest triplet substates, **I**, **II**, and **III**, and decay times of **1**. Adapted with permission from ref. 66. Copyright 2003, Elsevier.

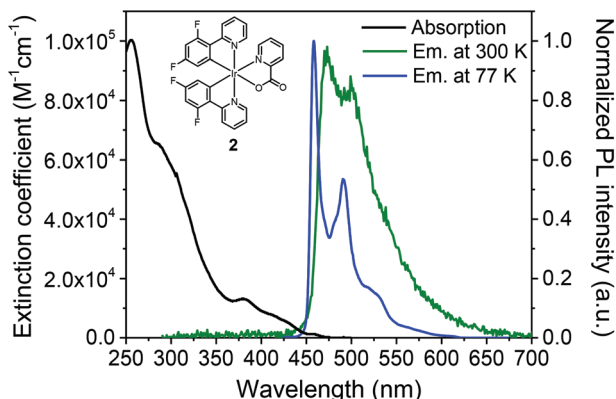


Fig. 5 Absorption and PL spectra of **2** in dichloromethane solution at RT and 77 K (inset: chemical structure of **2**).

researchers suggested that stronger vibrational coupling yields an increased NR decay rate and decreased PLQY. They estimated the vibrational coupling values using the Huang–Rhys factor,  $S_M$ , which roughly quantifies the structural distortion ( $\Delta Q$ ) of the excited state relative to the ground state.<sup>82,83</sup> If  $S_M = 0$ , the geometries of the excited and ground states should be identical, and only a sharp peak corresponding to the 0–0 transition should be observed. With increased  $\Delta Q$  and, hence, appearance of the 0–1 transition, the  $S_M$  value can be estimated using the intensity ratios of the 0–0 and 0–1 vibrational peaks:  $S_M = (I_{0-1}/I_{0-0})$ . Thus, higher  $S_M$  indicates increased vibrational coupling between the potential surfaces of the triplet excited state and the ground state; this yields lower PLQY as the transition probability is increased with increasing overlap between the initial and final states.

Samuel *et al.* also found that the experimental phosphorescence lifetime ( $\tau_P$ ) value of **4** (Fig. 6) in 2-methyl-tetrahydrofuran (2-MeTHF) increases from 0.9  $\mu$ s at 300 K to 2.2  $\mu$ s at 200 K and to 3.2  $\mu$ s at 77 K.<sup>81</sup> An Arrhenius plot showing the temperature-dependence of  $\tau_P$  gives activation energy of 0.27 eV (2178 cm<sup>-1</sup>). In the case of **5**,  $\tau_P$  changes from 0.15  $\mu$ s at 290 K to 3  $\mu$ s at 200 K, but is constant (3  $\mu$ s) at  $\leq 200$  K. The temperature-dependence of  $\tau_P$  gives an activation energy of

0.67 eV (5404 cm<sup>-1</sup>). On polymethyl methacrylate (PMMA) solid films, the emission decays of **3–5** (Fig. 6) reveal bi-exponential behaviour. The longer component for **5** increases from 1.35  $\mu$ s at 310 K to 3.7  $\mu$ s at 77 K, and the temperature dependence of  $\tau_P$  gives an activation energy of 0.13 eV (1049 cm<sup>-1</sup>); this is much smaller than that for the homogeneous solution in 2-MeTHF, as shown in Fig. 6. As the activation energies differ considerably between homogeneous solutions and solid films, they suggested that a vibronic-coupled NR decay mechanism could play an important role in lowering the PLQY. Such NR decay processes can be suppressed by employing rigid ligand frameworks.

We next consider, temperature-dependent NR decay processes, which occur for crossing from the emissive state to an upper non-emissive  $^3\text{MC}$  excited state. As the non-emissive  $^3\text{MC}$  states of cyclometalated Ir(III) complexes are high-energy, green and red phosphorescent Ir(III) complexes cannot access this state at RT. However, the upper-lying  $^3\text{MLCT}$  states of blue phosphorescent Ir(III) complexes can easily access this non-emissive  $^3\text{MC}$  state. In particular, Thompson *et al.* reported the generation of the  $^3\text{MC}$  state in blue phosphorescent Ir(III) complexes, **6–12**.<sup>84</sup> The temperature-dependences of  $\tau_P$  in 2-MeTHF reveal two different lower- and higher-temperature regions. These can be analysed according to the Boltzmann model eqn (1):

$$\tau_P = \frac{1}{k_{\text{obs}}} = \frac{\left\{ 1 + \exp\left(\frac{-E_1}{k_{\text{B}}T}\right) + \exp\left(\frac{-E_2}{k_{\text{B}}T}\right) \right\}}{\left\{ k_0 + k_1 \exp\left(\frac{-E_1}{k_{\text{B}}T}\right) + k_2 \exp\left(\frac{-E_2}{k_{\text{B}}T}\right) \right\}} \quad (1)$$

where,  $k_0$  is the decay rate from the lowest-energy triplet substate (**T<sub>1</sub>**),  $k_1$  and  $k_2$  are pre-exponential factors (decay rate constants),  $E_1$  and  $E_2$  are the activation energies for NR decay,  $k_{\text{B}}$  is the Boltzmann constant, and  $T$  is temperature in kelvin. In the lower-temperature region,  $k_1 = 10^5\text{--}10^6\text{ s}^{-1}$  and  $E_1 = 40\text{--}120\text{ cm}^{-1}$  were obtained; the latter corresponds to the ZFS energies between substates **I** and **III**. The NR decay at low temperatures proceeds from the non-emissive substate **III** populated from the emissive substate **I**. In the higher-temperature region,  $E_2$  values of  $4700 \pm 100$  (**6** and **7**),  $3400 \pm 100$  (**8** and **9**), and  $1600 \pm 100\text{ cm}^{-1}$  (**10–12**) were obtained, along with  $k_2$  values of  $4 \times 10^{14}$  (**6**),  $3.4 \times 10^{13}$  (**7**),  $5 \times 10^{12}$  (**8**),  $6.1 \times 10^{12}$  (**4**),  $1.2 \times 10^{12}$  (**10**),  $2.6 \times 10^{11}$  (**11**), and  $3.7 \times 10^9\text{ s}^{-1}$  (**12**). The NR decay in the high-temperature region was attributed to crossing from the emissive lowest triplet state to the non-emissive  $^3\text{MC}$  state. The argument for this mechanism is supported by  $(E_{0-0} + E_2) = 25\,680\text{--}27\,370\text{ cm}^{-1}$  for **6–11**, respectively (corresponding to 74–76 kcal mol<sup>-1</sup>), which are close to the dissociation energies of Ir-ligand bonds. The large  $k_2$  values, which are associated with high-frequency vibrations accompanied by bond breaking, also support this interpretation. Based on the ‘Energy-Gap Law’, the  $k_{\text{nr}}$  value for vibration-coupled deactivation has been estimated as  $4 \times 10^3\text{ s}^{-1}$ , sufficiently low for a minor impact of vibration-coupled decay on the net NR decay. Accordingly, the authors concluded that NR decay rates can be decreased and PLQY can be

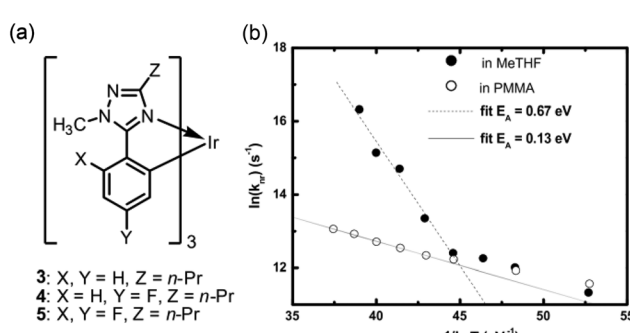


Fig. 6 (a) Chemical structures of **3–5** and (b) Arrhenius (activation energy) plot of **5** dissolved in 2-MeTHF or solid PMMA host. Adapted with permission from ref. 81. Copyright 2008, Elsevier.

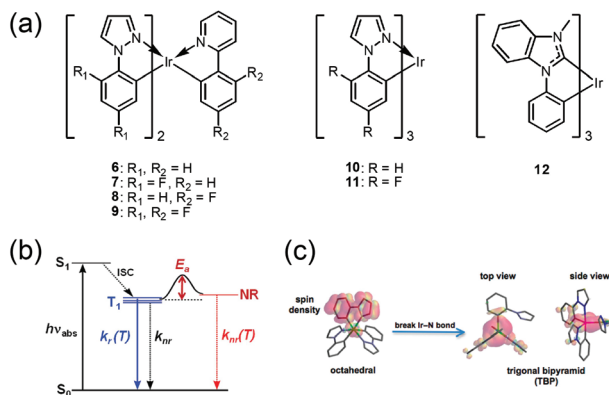


Fig. 7 (a) Chemical structures of **6–12**. (b) Three types of decay process from  $T_1$  state to the ground state: temperature-dependent radiative process,  $k_r(T)$ , or one of two NR decay processes. (c) Changes in chemical structures and spin density surfaces calculated for triplet states of six- and five-coordinated forms of **10**. Adapted with permission from ref. 84. Copyright 2009, American Chemical Society.

improved by increasing the energy separation between the emissive and non-emissive states. In addition, on the basis of a DFT calculation for **10**, they propose a change from the 6-coordinated lowest triplet state to the  $^3\text{MC}$  state with a 5-coordinated trigonal bipyramidal structure accompanied by rupturing of one Ir–N bond, as shown in Fig. 7. Later, structural change in the excited state is supported by theoretical calculations, which showed a lengthened Ir–N bond up to 2.70 Å in the  $^3\text{MC}$  state due to the strong  $\sigma$ -antibonding interactions between the metal and the N atom in the ppy ligand.<sup>85</sup>

Haga *et al.* reported a similar phenomenon in Ir(III) complexes with tridentate pyrazolyl ligands, **13** and **14**.<sup>86</sup> The intense absorptions at 320–400 nm and weak bands at >410 nm were attributed to the  $^1\text{MLCT}$  transition and  $^3\text{LC}$  mixed with  $^3\text{MLCT}$  transitions, respectively. In those complexes, the emission spectra at 77 K are highly structured, with the 0–0 vibration band being highest; this is characteristic of emission from a  $^3\text{LC}$ -dominated state with a minor  $^3\text{MLCT}$  contribution. The emission behaviour is highly temperature-dependent, as revealed by the shift from considerably short lifetimes (0.18–140 ns) at 298 K to much longer lifetimes (3.9–13.1  $\mu$ s) at 77 K. The temperature dependence of  $\tau_p$  for **13** at 90–300 K reveal biphasic behaviour, which was analysed based on the following bi-exponential eqn (2):

$$k_d(T) = A_1 \exp\left(\frac{-E_1}{k_B T}\right) + A_2 \exp\left(\frac{-E_2}{k_B T}\right) \quad (2)$$

where  $k_d(T)$  is the temperature-dependent decay rate, and  $A_1$  and  $A_2$  are pre-exponential frequency factors. Data fitting gave  $A_1 = 2.3 \times 10^{13} \text{ s}^{-1}$ ,  $E_1 = 1720 \text{ cm}^{-1}$ ,  $A_2 = 3.5 \times 10^5 \text{ s}^{-1}$ , and  $E_2 = 27 \text{ cm}^{-1}$ . The values of  $A_1$  and  $E_1$  are very similar to those reported for  $[\text{Ru}(\text{terpyridine})_3]^{2+}$  ( $2.3 \times 10^{13} \text{ s}^{-1}$  and  $1680 \text{ cm}^{-1}$ ), which were assigned as the parameters for crossing from  $^3\text{MLCT}$  to  $^3\text{MC}$ .<sup>87</sup> The much lower  $E_2$  value was attributed to the ZFS. Furthermore, the low  $A_1$  was discussed in

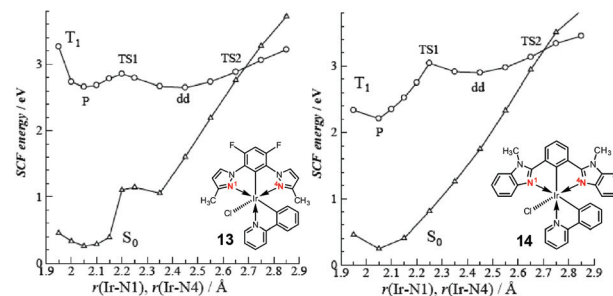


Fig. 8 Potential-energy curves involving thermal deactivation of phosphorescent state (P) calculated as function of bond length  $\text{Ir-N(1)}$  ( $\text{Ir-N(4)}$ ) for **13** and **14**. Adapted with permission from ref. 86. Copyright 2008, American Chemical Society.

terms of the non-adiabatic transition from the triplet state to the ground state with unfavourable vibrational function overlapping. The excited-state potential surfaces for the non-emissive **13** and highly emissive **14** were compared at the unrestricted DFT level; the results are depicted in Fig. 8. In the case of **13**, the phosphorescent state (P) and non-emissive  $^3\text{MC}$  states are similar in energy and separated by a low barrier ( $P \rightarrow \text{d-d state, TS1, } 0.2 \text{ eV}$ ). In the case of **14**, however, the  $^3\text{MC}$  minimum is located at a potential that is 0.7 eV higher than P. Hence, TS1 and TS2 ( $\text{d-d state} \rightarrow \text{ground state}$ ) are substantially enlarged, such that they eventually inhibit crossing to the  $S_0$  surface via  $^3\text{MC}$  at RT. The TS1 and TS2 calculated for **13** were  $1600$  and  $1800 \text{ cm}^{-1}$ , respectively, very similar to the experimental value of  $E_1$  ( $1720 \text{ cm}^{-1}$ ). Surface crossing from P to  $^3\text{MC}$  requires movement of the excited electron in the  $\pi^*$  of the ppy ligand to the  $\text{d}-\sigma^*$  orbital, a transition forbidden by the orbital orthogonality for the octahedral structure. To allow crossing from P to  $^3\text{MC}$  state, orbital mixing in TS1 is assumed to occur through twisting of the pyrazolyl rings of **13**. Therefore, retardation of the  $^3\text{MC}$  state generation would be beneficial as regards increased efficiency for cyclometalated Ir(III) complexes. Available photophysical- and electrochemical data of **1–14** with their device performances are summarised in Table 1. In the following, reported strategies for tuning the emission colours of cyclometalated Ir(III) complexes to higher energies and for enhancing their efficiencies are summarised.

### 3. Design of blue-emissive Ir(III) complex

#### 3.1. Introducing F atom(s) to cyclometalating ligand

**3.1.1. Homoleptic complexes.** The most common strategy for achieving blue-shifted emission of cyclometalated Ir(III) complexes may be introduction of electron-withdrawing groups (EWGs) to the phenyl ring of a cyclometalated ligand. Computational investigation of **1** revealed that the HOMO is mainly localised at the Ir d-orbital and phenyl moiety, and the LUMO is localised at the pyridyl moiety.<sup>55</sup> Therefore, introducing EWGs to the phenyl ring allows stabilisation of the

Table 1 Available photophysical- and electrochemical data of 1–14 with their device performances

	Photophysical properties					Device performances				Ref.
	$\lambda_{\text{em}}$ (nm)	$\tau_{\text{em}}$ (μs)	PLQY	$k_{\text{r}}$ (s <sup>-1</sup> )	$k_{\text{nr}}$ (s <sup>-1</sup> )	Oxidation (V)	EL ( $\lambda_{\text{max}}$ , nm)	CIE (x, y)	EQE <sub>max</sub> (%)	
<b>1</b>	510	1.9	0.40	$2.1 \times 10^5$	$3.2 \times 10^5$	0.31	—	—	—	9
	—	—	—	—	—	—	518	(0.30, 0.63)	14.3	160
	514	—	—	—	—	—	510	(0.28, 0.63)	5.7	88
<b>2</b>	471, 495	1.74	0.94	$5.5 \times 10^5$	$0.3 \times 10^5$	—	—	(0.15, 0.36)	5.1	174
<b>3</b>	449, 479	1.08	0.66	$6.1 \times 10^5$	$3.1 \times 10^5$	0.28	—	—	—	80 and 96
<b>4</b>	428, 456	1.25	0.27	$2.2 \times 10^5$	$5.8 \times 10^5$	0.50	—	—	—	80 and 96
<b>5</b>	425, 450	0.15	0.03	$2.0 \times 10^5$	$6.5 \times 10^6$	0.72	—	—	—	80 and 96
<b>6</b>	500	1.7	0.95	$5.6 \times 10^5$	$0.3 \times 10^5$	—	—	—	—	84
<b>7</b>	475	2.6	0.93	$3.6 \times 10^5$	$0.3 \times 10^5$	—	—	—	—	84
<b>8</b>	500	1.2	0.55	$4.6 \times 10^5$	$3.8 \times 10^5$	—	—	—	—	84
<b>9</b>	457	1.3	0.60	$4.6 \times 10^5$	$3.1 \times 10^5$	—	—	—	—	84
<b>10</b>	412 <sup>a</sup>	0.002	<0.01	—	—	—	—	—	—	84
<b>11</b>	388 <sup>a</sup>	0.007	<0.01	—	—	—	—	—	—	84
<b>12</b>	382	1.1	0.37	$1.1 \times 10^5$	$3.4 \times 10^5$	—	—	—	—	84
<b>13</b>	456 <sup>a</sup>	0.0002	<0.001	—	—	0.75	—	—	—	86
<b>14</b>	555	1.78	0.78	$4.4 \times 10^5$	$1.2 \times 10^5$	0.42	—	—	—	86

<sup>a</sup> Measured at 77 K.

HOMO energy level. Furthermore, decoration of the pyridyl unit with an electron-donating group can heighten the LUMO energy level. For example, Thompson *et al.* reported that introduction of F atoms at positions 4- and 6- on the **1**, with the resultant complex being named *fac*-Ir(dfppy)<sub>3</sub> (**15**, Fig. 9), significantly shifts the emission from 510 to 468 nm, with similar PLQY (0.43) and emission lifetime ( $\tau_{\text{em}} = 1.6 \mu\text{s}$ ).<sup>9</sup> Those researchers also reported that the *mer*-isomers can undergo thermal conversion to *fac*-isomers, as the former and latter are kinetically and thermodynamically favoured products, respectively.

In 2006, De Cola *et al.* explored the number of F atoms in the same molecular architecture.<sup>89</sup> When one more F atom is substituted at the 3-position of the phenyl ring, (**16**, Fig. 9), the emission shows a hypsochromic shift to 459 nm. Interestingly,

however, the emission of the tetra-fluorinated complex (**17**, Fig. 9), shifts to lower energy at 468 nm. De Cola *et al.* suggested that the lower emission energy of **17** is due to the more positive reduction potentials caused by the presence of more F atoms. Note also that these two complexes have different emission quantum yields (0.30 and 0.53 for **16** and **17**, respectively) and  $\tau_{\text{em}}$  at RT (1600 and 2300 ns for **16** and **17**, respectively). The highest EQE value of 5.5% was observed for an electroluminescent device containing **17**. Those authors also observed different stabilities for devices fabricated with the *fac*- and *mer*-isomers. That is, the latter exhibited fast spectral changes in emission from the blue to green region of the spectrum.

Further theoretical studies, performed by Tian *et al.* in 2011 revealed that the differences between **16** and **17** are due to the

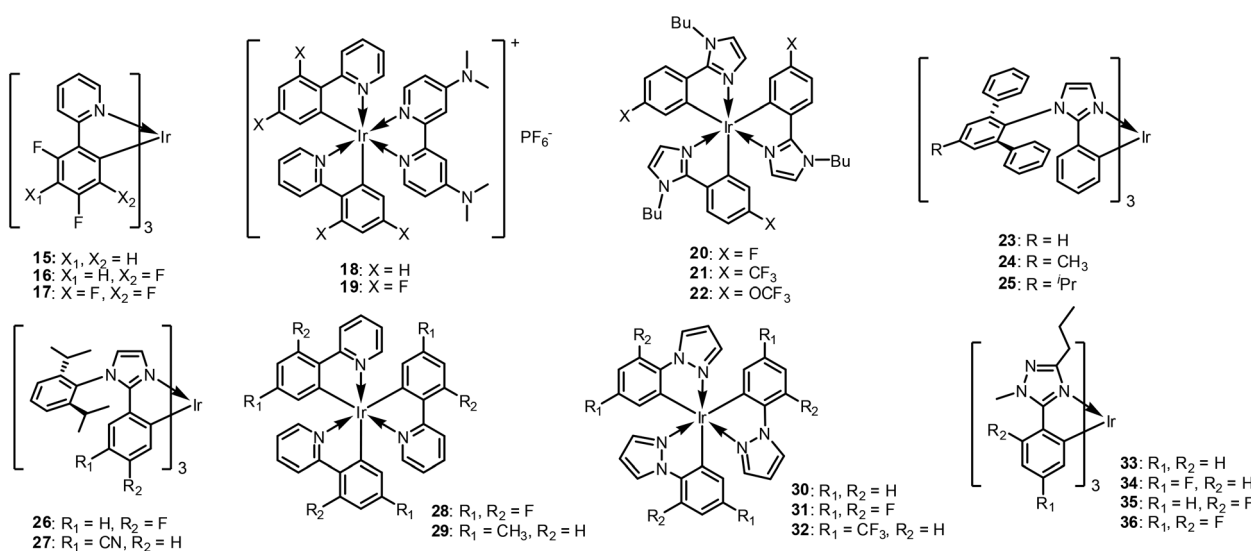


Fig. 9 Chemical structures of F-containing blue-emissive homoleptic Ir(III) complexes, 15–36.

different transition dipole moments.<sup>90</sup> The same effects were also observed for cationic Ir(III) complexes. De Angelis *et al.* reported a combined experimental and theoretical study comparing **18** (a dfppy-based complex) and **19** (a ppy-based complex, see Fig. 9).<sup>91</sup> Those authors controlled the phosphorescent emission wavelength and improved the quantum yields by modulating the electronic structures of the cyclometalated Ir(III) complexes through F functionalisation. The F-functionalised **19** showed blue-shifted emission at 463 nm with a higher PLQY (0.85) than **18** ( $\lambda_{\text{max}} = 491$  nm, PLQY = 0.80) in acetonitrile solution. This was related to a dramatic decrease in the NR deactivation rate constant, in agreement with the 'Energy-Gap Law'. The  $\tau_{\text{em}}$  values were also found to increase from **18** (2.4  $\mu\text{s}$ ) to **19** (4.1  $\mu\text{s}$ ), yielding an overall reduction in the  $k_{\text{r}}$ ; this suggests increasing  $\pi$ - $\pi^*$  character in the emitting excited states. DFT and TD-DFT calculations with solvent effects were conducted to characterise the lowest triplet excited states and revealed that the extensive mixing of the  $^3\text{MLCT}$  and  $\pi$ - $\pi^*$  contributions agrees with the  $\tau_{\text{em}}$  increment for **19** compared to **18**.

Other modifications were made by replacing phenyl pyridine ligands with phenyl heterocyclic ring systems, such as imidazole, pyrazole, and triazole. Note that imidazole-based homoleptic Ir(III) complexes have been used as blue dopants because the imidazole group can heighten the LUMO energy level, thereby enlarging the energy gap and increasing the  $T_1$  energy level. Kitamura *et al.* reported homoleptic and heteroleptic Ir(III) tirs(phenylimidazolinate) complexes.<sup>92</sup> Upon replacement of the pyridyl ring with the imidazolyl ring, the LUMO mainly populates the phenyl ring; this is quite different from the LUMOs of ppy-based Ir(III) complexes. Accordingly, substitution of an F atom into the phenyl ring (**20**, Fig. 9) yields the most blue-shifted emission of 453 nm at RT (PLQY = 0.60), with a value of 446 nm at 77 K. In this case,  $\pi$ -electron-donating substituents can induce a blue-shift of the emission spectra. They fabricated an OLED device using **22**, which exhibited efficient luminescence compared with a **1**-based device. The two devices showed similar emission colours, but the emission luminance of the former was smaller ( $L_{\text{max}} = 889$  cd m<sup>-2</sup> at 15 V compared to  $L_{\text{max}} = 3490$  cd m<sup>-2</sup> at 13 V), because of inefficient carrier injection into the emitting layer.

Kang *et al.* also studied imidazole-based Ir(III) complexes, but with a bulky terphenyl unit on the N atom of the imidazolyl ring, (**23**–**25**, Fig. 9).<sup>93</sup> Those researchers concluded that a terphenyl ligand without alkyl chains (**23**) is advantageous in terms of lifetime, whereas the terphenyl with alkyl chains (**24**, **25**) is efficient in terms of PLQY. When employed in OLED devices, the EQEs of **24** and **25** were 21.1% and 21.3%, respectively, which were higher than that of **23** (19.2%). The authors explained that the high PLQYs of **24** and **25** assisted the triplet emission of the blue devices by effectively harvesting triplet excitons.

In 2018, Lee *et al.* reported diisopropylphenyl-functionalised phenylimidazole-based Ir(III) complexes (rather than a terphenyl group) (**26** and **27**, Fig. 9), which showed more blue-shifted emission at 454 nm.<sup>94</sup> Even though the diisopropyl-

phenyl group has lesser bulkiness than the terphenyl ring, this group still efficiently limits intermolecular aggregation and prevents the different self-quenching processes. Substitution of CN at position-5 (**27**), was found to significantly affect the device lifetime; a longer device lifetime exceeding 550 h at 200 cd m<sup>-2</sup> was obtained, with EQE<sub>max</sub> = 17.6% and CIE (0.15, 0.28).

Pyrazole-attached Ir(III) complexes were also investigated. For example, Thompson *et al.* reported that the MLCT transitions of the pyrazolyl-based complexes, **30**–**32** (Fig. 9) are hypsochromically shifted relative to pyridyl-based complexes (**1**, **28**, and **29**), due to the higher triplet energy of phenylpyrazole (3.28 eV) compared to ppy (2.88 eV).<sup>9</sup> F substitution effectively shifts the emission further to the blue region, up to 21 nm. Notably, phosphorescence of **31** was observed at 390 nm, which has very rarely been reported to date. However, these homoleptic pyrazolyl-based complexes are not emissive at the RT. Therefore, pyrazolyl-based ligands tend to be used in heteroleptic rather than homoleptic systems (*vide infra*).

Samuel *et al.* previously reported a series of phenyl triazole-type Ir(III) complexes.<sup>80</sup> As triazole has a higher LUMO energy than pyridine,<sup>95</sup> replacement of the pyridyl moiety with a triazolyl ring was expected to shift the emission further to the blue region than that of the corresponding ppy-based Ir(III) complex. As expected, **6** has  $\lambda_{\text{max}}$  at 449 nm, which is significantly blue shifted compared to that of **1** ( $\lambda_{\text{max}} = 510$  nm). Ir(III) complexes with F atom(s) **6**–**8** show hypsochromically shifted emissions relative to non-F-based complexes, by up to 425 nm. However, the PLQYs decrease with increased F atoms. This is because of the increased ligand triplet energy in the emissive energy state, which decreases the material radiative decay rate through vibronic-coupled NR decay, as explained in the previous section.

Powell *et al.* theoretically studied the effects of fluorination on the role of metal-ligand bond fission in the NR decay of excited states in cyclometalated Ir(III) complexes.<sup>26,96</sup> The calculated activation barrier to the  $^3\text{MC}$  state shows a clear correlation with the experimentally obtained NR decay rate for a series of Ir(III) complexes. As  $^3\text{MC}$  state formation requires breaking of an Ir–N bond, Powell *et al.* compared Ir–N bond distances in the  $^3\text{MC}$  states of cyclometalated Ir(III) complexes. For **33** and **34** (Fig. 9), the Ir–N bond length changes in the  $^3\text{MC}$  state relative to the ground-state structure are much smaller than those of **35** and **36** (Fig. 9). Accordingly, the activation barrier to the  $^3\text{MC}$  state is lower for **35** and **36**, which yields low PLQY.

Samuel *et al.* extended their work to dendronised triazole-based Ir(III) complexes, to attain a solution-processable material.<sup>97–99</sup> F-Attached dendrimers **38**–**40** (Fig. 10) show phosphorescence emissions at approximately 441 nm; however, these materials are unsuitable for device applications because of their low triplet energy and vibrational quenching, which yield luminescence quenching or low thermal properties.<sup>97,98</sup> To solve this problem, dendrons were later modified to have a twisted geometry and successfully utilised in a blue PH-OLED device.<sup>99</sup> Dendrimer **41** shown in Fig. 10 is

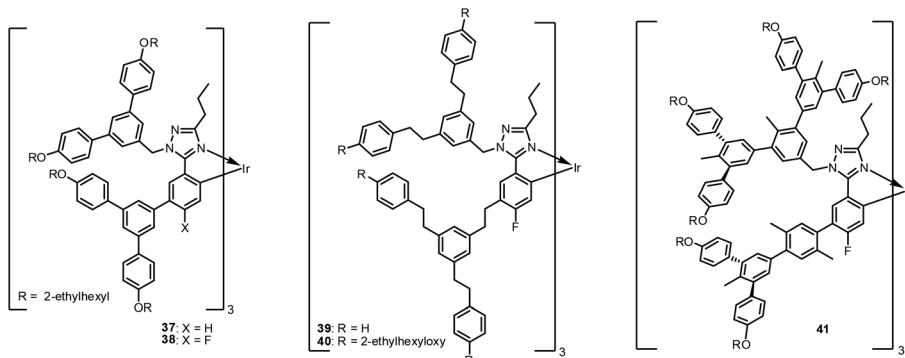


Fig. 10 Structures of dendritic blue emissive Ir(III) complexes, 37–42.

highly emissive, with PLQY = 0.94 and 0.6, and  $\tau_{\text{em}}$  of 3.6 and 2.8  $\mu\text{s}$ , in solution and neat film, respectively. Its high emissivity is attributed to the dendron rigidifying effect, which reduces the geometry change in the excited state. Using 41, Samuel *et al.* fabricated a preliminary OLED device and showed EQE<sub>max</sub> of 3.9% with CIE coordinates of (0.16, 0.17). Dendritic approaches are still being investigated, especially for solution-processed phosphorescent OLEDs.<sup>100–106</sup> Available photophysical- and electrochemical data of 15–41 with their device performances are summarised in Table 2.

**3.1.2. Heteroleptic complexes.** Based on the same strategy, heteroleptic systems have also been developed. For example, 2, which is a heteroleptic Ir(III) complex having a cyclometalated 4,6-difluorophenyl pyridine (dfppy) ligand as the main ligand and a picolinate ligand as an ancillary ligand, has been widely utilised as a blue-emissive heteroleptic Ir(III) complex.<sup>10,105</sup> Indeed, 2 may be the most widely used blue emitter because of its good device performance, simple molecular structure, and ease of synthesis. However, 2 is not authentic blue but, rather, greenish-blue in both energy ( $\lambda_{\text{max}} = 468$  nm) and colour. It has a CIE of (0.17, 0.34), which corresponds to sky blue,<sup>105</sup> far from that required for a full-colour display. Thus, many refinements towards development of a deeper-blue-emissive cyclometalated Ir(III) complex have been implemented, by replacing the picolinate ligand with other ancillary ligands.

Thompson *et al.* reported photophysical and electrochemical properties of nineteen cyclometalated Ir(III) complexes with various ancillary ligands and three types of main ligand (dfppy, ppy, and terpyridine (tpy)).<sup>106</sup> The ancillary ligands were chosen to be ‘non-chromophoric’, so as to drive the excited-state properties dominated by the main ligands and Ir. For this approach, the  $^3\text{LC}$  state energy was expected to be relatively constant for all complexes, whereas the  $^1\text{MLCT}$  state energies could be altered by varying the ancillary ligand. As expected, the F-substituted main ligand (dfppy) showed a blue-shifted emission relative to the tpy-based Ir(III) complex. The effects of the ancillary ligands on the excited-state properties of the cyclometalated Ir(III) complexes were independent of the choice of main ligand. That is, the cyclometalated Ir(III) complexes with the same ancillary ligands but different main ligands exhibited different  $k_{\text{r}}$  values. Thompson *et al.*

explained that the degree of  $^1\text{MLCT}$  character mixed into the  $\text{T}_1$  state decreases when the Ir(III) complex has a deeper HOMO energy level. This yields an increased energy gap between the singlet and triplet energies and consequently, lowers the  $k_{\text{r}}$  values.

De Cola *et al.* studied triazole-based ancillary ligand systems, 42–48, as described in Fig. 11.<sup>107</sup> Those researchers designed ppy main ligands while varying the phenyl-ring substitution positions at 4/6 or 5 with different substituents, *i.e.*, H, F, and  $\text{CF}_3$ . The ancillary ligands were based on phenyltriazole with substituent variations at the triazole ring positions. They performed a detailed theoretical analysis of the effects of the substituents in the main ligand to study the emissive state properties. Calculation results showed that the substituents not only affect the emission energy but, also, change the ordering of the lowest excited triplet states. The same group reported a series of heteroleptic Ir(III) complexes, 45, 48, and 49–54 (Fig. 11), in which the 1,2,4-triazole ancillary ligands are varied with different substituents while the main ligand is fixed as dfppy.<sup>108</sup> By increasing the electron-withdrawing ability, the HOMO energy level is lowered, and consequently, the HOMO–LUMO gap is widened. This yields blue-shifted emission with narrower full width at half maximum. In this series, complexes 51 and 52 exhibit lower PLQY, which may be due to the torsional angle between the phenyl and triazole rings arising from F atoms in the *ortho* position. In these cases, the lowest MLCT states are shifted from the pyridyl-triazole to the ppy. Two preliminary devices were constructed using 49 and 51, with both exhibiting EQEs exceeding 7% together with a blue colour (CIE<sub>x,y</sub> = 0.17, 0.27). De Cola *et al.*’s work was extended to 1,2,3-triazole-based Ir(III) complexes, 55–57 (Fig. 11).<sup>109</sup> The emission spectra in the solution for 1,2,3-triazole-based complexes are slightly blue-shifted with respect to their analogous complexes with 1,2,4-triazole moieties, 45, 48, and 49–54, having enhanced colour purity to blue.

Bryce *et al.* introduced F-substituted 2,3'-bipyridine derivatives rather than ppy derivatives as the main ligand, to lower the HOMO level and develop efficient deep-blue phosphors, *i.e.*, 58 and 59 (Fig. 11).<sup>110</sup> Both of these complexes show intense blue phosphorescence emission at 437 and 435 nm,

Table 2 Available photophysical- and electrochemical data of 15–41 with their device performances

	Photophysical properties					Device performances				Ref.
	$\lambda_{\text{em}}$ (nm)	$\tau_{\text{em}}$ (μs)	PLQY	$k_r$ (s <sup>-1</sup> )	$k_{\text{nr}}$ (s <sup>-1</sup> )	Oxidation (V)	EL ( $\lambda_{\text{max}}$ , nm)	CIE (x, y)	EQE <sub>max</sub> (%)	
15	468	1.6	0.43	$2.7 \times 10^5$	$3.6 \times 10^5$	0.78	—	—	—	9
	495	—	0.06	—	—	—	—	(0.27, 0.38)	0.6	88
16	459, 486	0.1	0.03	$1.9 \times 10^5$	$4.4 \times 10^5$	—	—	—	—	89
17	468, 497	0.1	0.03	$2.3 \times 10^5$	$2.0 \times 10^5$	—	478, 511	—	3.2	89
18	491, 520	2.4	0.80	$3.3 \times 10^5$	$0.8 \times 10^5$	0.72	—	—	—	91
19	463, 493	4.1	0.85	$2.1 \times 10^5$	$0.4 \times 10^5$	1.00	—	—	—	91
20	453, 482	3.4	0.60	$1.7 \times 10^5$	$1.2 \times 10^5$	—	—	—	—	92
21	486, 518	2.8	0.40	$1.4 \times 10^5$	$2.1 \times 10^5$	—	—	—	—	92
22	461, 492	3.3	0.53	$1.6 \times 10^5$	$1.4 \times 10^5$	—	464, 494	(0.23, 0.35)	—	92
23	463, 487	—	0.38	—	—	—	—	(0.17, 0.30)	19.2	93
24	459, 487	—	0.45	—	—	—	—	(0.17, 0.28)	21.1	93
25	462, 487	—	0.50	—	—	—	—	(0.17, 0.29)	21.3	93
26	454, 484	1.1	0.87	$7.9 \times 10^5$	$1.2 \times 10^5$	—	455, 484	(0.17, 0.30)	18.9	94
27	462, 494	1.8	0.99	$5.5 \times 10^5$	$0.5 \times 10^4$	—	462, 494	(0.15, 0.28)	22.5	94
28	468	1.6	0.05	$2.7 \times 10^5$	$3.6 \times 10^5$	0.78	—	—	—	9
29	510	2.0	0.50	$2.5 \times 10^5$	$2.5 \times 10^5$	0.30	—	—	—	9
30	414 <sup>a</sup>	14 <sup>a</sup>	—	—	—	0.39	—	—	—	9
31	390 <sup>a</sup>	27 <sup>a</sup>	—	—	—	0.80	—	—	—	9
32	428	0.05	—	—	—	0.73	—	—	—	9
33	449	1.08	0.66	$6.1 \times 10^5$	$3.1 \times 10^5$	0.28	—	—	—	96
34	443	0.15	0.06	$4.0 \times 10^5$	$6.3 \times 10^5$	0.50	—	—	—	96
35	428	1.25	0.27	$2.2 \times 10^5$	$5.8 \times 10^6$	0.50	—	—	—	96
36	425	0.15	0.03	$2.0 \times 10^5$	$6.5 \times 10^6$	0.72	—	—	—	96
37	468, 495	2.8	0.76	$2.7 \times 10^5$	$0.9 \times 10^5$	0.31	—	(0.18, 0.35)	7.9	98
38	441, 468	22.0	0.59	$0.3 \times 10^5$	$0.2 \times 10^5$	0.53	—	—	—	97 and 99
39	441, 468	1.7	0.46	—	—	0.47	—	—	—	98 and 99
40	441, 470	1.7	0.45	$2.7 \times 10^5$	$3.3 \times 10^5$	0.45	—	—	—	98 and 99
41	435, 465	3.6	0.94	$2.6 \times 10^5$	$1.7 \times 10^4$	0.61	438, 466	(0.16, 0.16)	3.9	99

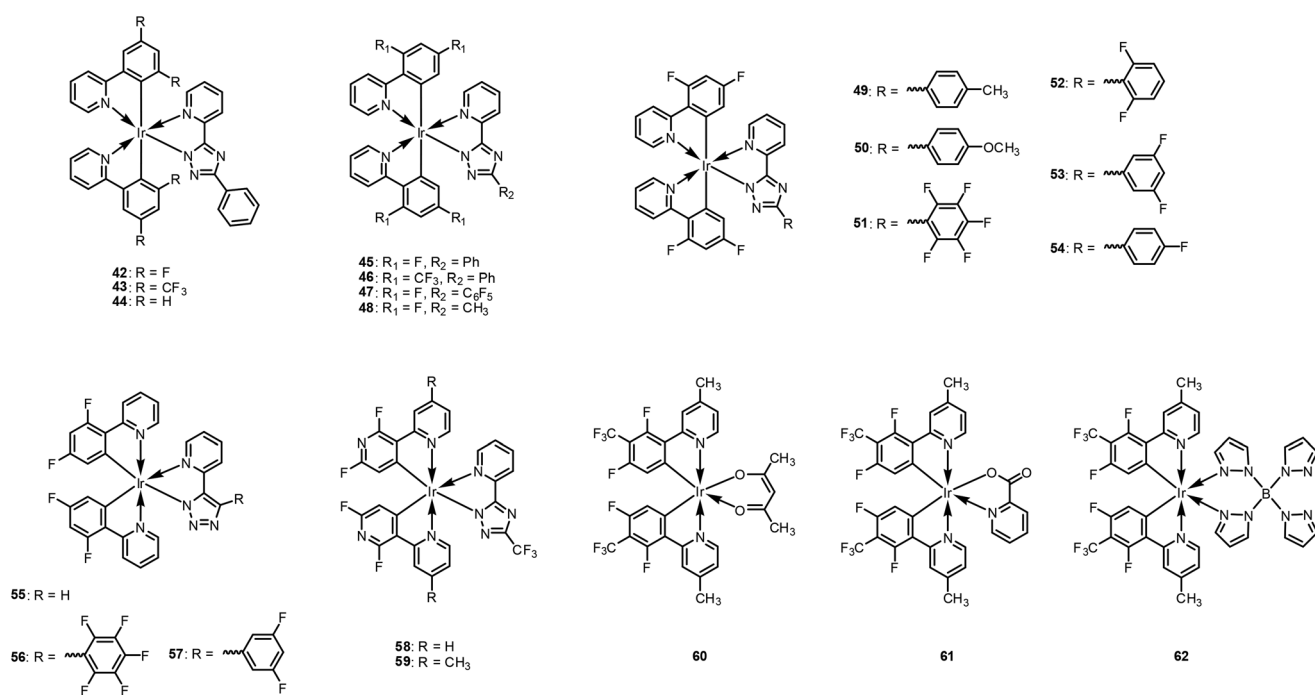
<sup>a</sup> Measured at 77 K.

Fig. 11 Chemical structures of heteroleptic Ir(III) complexes, 42–62.

respectively, with high PLQYs exceeding 0.65. When implemented in OLED devices, the **59**-based device exhibited 13% EQE with a deep blue colour ( $CIE_{x,y} = 0.16, 0.17$ ).

Recently, our group investigated the role of the ancillary ligand on the emission behaviours.<sup>111</sup> A series of heteroleptic Ir(III) complexes, **60**–**62**, were prepared, comprised of 2-(2,4-difluoro-3-(trifluoromethyl)phenyl)-4-methylpyridine (dfCF<sub>3</sub>) as the main ligand and the following different ancillary ligands: acetylacetone (**60**), picolinate (**61**), and tetrakis-pyrazolyl borate (**62**). The heteroleptic Ir(III) complexes of **60**–**62** exhibit emission peaks at 470, 455, and 450 nm, respectively, in dichloromethane solution. For **60**–**62**, the Huang–Rhys factors are estimated to be 0.76, 0.87, and 0.97, respectively, as shown in Fig. 12a. Interestingly, however, the NR rate constants are in the order **60** ( $4.89 \times 10^5 \text{ s}^{-1}$ ) > **61** ( $1.17 \times 10^5 \text{ s}^{-1}$ ) > **62** ( $0.28 \times 10^5 \text{ s}^{-1}$ ). To explain this phenomenon, we measured the temperature-dependent  $\tau_{\text{em}}$  to estimate the activation barrier from the radiative triplet state to NR state, <sup>3</sup>MC. The activation barriers were calculated as 46, 61, and >100 meV for **60**–**62**, respectively. Theoretical quantum chemical calculations were also conducted to support the experimental data. According to these calculations, the activation barrier for **62** (7.9 kcal mol<sup>-1</sup>) is significantly higher than those of **60** (1.7 kcal mol<sup>-1</sup>) and **61** (2.9 kcal mol<sup>-1</sup>), as depicted in

Fig. 12b. We suggested that reorganisation to a trigonal bipyramidal geometry may be difficult because of the steric demands of the borate ligand. Further, the bulkiness of the borate ligand may restrict the free rotation of the pyrazolyl group. Thus, the activation barrier to <sup>3</sup>MC for **62** is much higher than those of **60** and **61**. Accordingly, a **62**-based blue phosphorescent OLED device exhibited the best performance among the series, with high current and power efficiencies of  $32.9 \text{ cd A}^{-1}$  and  $25.4 \text{ lm W}^{-1}$ , respectively. Available photophysical- and electrochemical data of **49**–**62** with their device performances are summarised in Table 3.

**3.1.3. Alternate EWGs.** However, limitations regarding the long-term device stability arise for F-substituted cyclometalating ligands. Cleavage of the aromatic C–F bond of **2** during OLED operation, confirmed by electron spray ionisation mass spectrometry, has been reported.<sup>112</sup> The researchers suggested two important degradation mechanisms for **2**: (1) cleavage of an F atom may generate a significant change in the emission wavelength, and (2) the cleavage product may undergo further chemical reactions with other organic materials. Accordingly, other types of electron-withdrawing groups have been utilised to replace the F atom, for example, the cyano,<sup>93,113–115</sup> trifluoromethyl,<sup>116–121</sup> and sulfonyl<sup>122–126</sup> groups.

### 3.2. Strategies for retarding the NR decay process

As deep-blue-emitting compounds have high-energy  $T_1$  states, the <sup>3</sup>MC state, which is a NR state, can be generated using relatively small thermal energies, as described above. Generation of this NR state not only decreases the PLQY, but also promotes electrons into metal–ligand  $\sigma^*$  orbitals. The latter induces deformation of the Ir–N bond that limits photostability and causes device efficiency degradation.<sup>127</sup> Therefore, strategies to retarding <sup>3</sup>MC state generation for deep-blue emissive cyclometalated Ir(III) complexes are necessary. Note that the modification must only affect the <sup>3</sup>MC state and not the frontier orbitals, which are involved in the luminescent  $T_1$  state. The following are some strategies developed for this purpose.

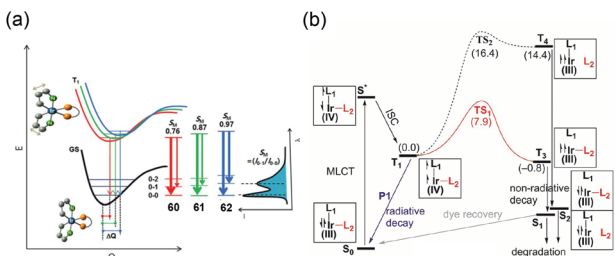


Fig. 12 (a) Energy potential curves with Huang–Rhys factors for **60**–**62** and (b) reaction profiles for Ir–N bond cleavage to form NR states for **62**. Adapted with permission from ref. 111. Copyright 2009, The Royal Society of Chemistry.

Table 3 Available photophysical- and electrochemical data of **49**–**62** with their device performances

Photophysical properties					Device performances					
$\lambda_{\text{em}}$ (nm)	$\tau_{\text{em}}$ (μs)	PLQY	$k_r$ (s <sup>-1</sup> )	$k_{\text{nr}}$ (s <sup>-1</sup> )	Oxidation (V)	EL ( $\lambda_{\text{max}}$ , nm)	CIE ( $x, y$ )	$\text{EQE}_{\text{max}}$ (%)	Ref.	
<b>49</b>	463, 492	0.1	$2.0 \times 10^5$	$2.8 \times 10^5$	0.91	—	—	—	108	
<b>50</b>	464, 492	0.1	$0.01$	$1.2 \times 10^5$	$0.8 \times 10^5$	0.91	—	—	108	
<b>51</b>	458, 487	0.2	0.04	$3.0 \times 10^5$	$1.6 \times 10^6$	1.02	461, 490	(0.17, 0.27)	7.4	108
<b>52</b>	460, 490	0.1	0.04	$2.7 \times 10^5$	$1.4 \times 10^6$	0.99	—	—	108	
<b>53</b>	459, 488	0.2	0.04	$2.9 \times 10^5$	$7.1 \times 10^5$	0.99	—	—	108	
<b>54</b>	459, 489	0.1	0.03	$2.1 \times 10^5$	$4.2 \times 10^5$	0.97	—	—	108	
<b>55</b>	460, 489	1.2	0.32	$2.6 \times 10^5$	$5.6 \times 10^5$	0.98	495	(0.18, 0.40)	0.4	109
<b>56</b>	457, 487	1.3	0.32	$2.3 \times 10^5$	$5.3 \times 10^5$	1.02	—	—	—	109
<b>57</b>	458, 487	1.1	0.27	$2.5 \times 10^5$	$6.8 \times 10^5$	0.99	495	(0.17, 0.40)	0.48	109
<b>58</b>	437, 466	3.0	0.65	$2.2 \times 10^5$	$1.2 \times 10^5$	—	430–440	(0.15, 0.13)	11.2	110
<b>59</b>	435, 464	3.0	0.70	$2.3 \times 10^5$	$1.0 \times 10^5$	—	460–470	(0.14, 0.11)	13.0	110
<b>60</b>	470, 494	0.9	0.56	$6.2 \times 10^5$	$4.9 \times 10^5$	0.88	—	(0.14, 0.26)	19.9	111
<b>61</b>	455, 484	1.8	0.79	$4.4 \times 10^5$	$1.2 \times 10^5$	1.12	—	(0.14, 0.18)	15.5	111
<b>62</b>	450, 478	4.6	0.87	$1.9 \times 10^5$	$0.3 \times 10^5$	1.18	—	(0.14, 0.20)	22.6	111

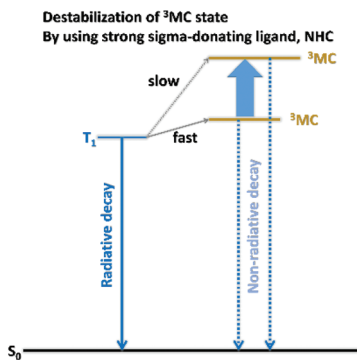


Fig. 13 Effect of NHC ligand on destabilisation of non-emissive state ( ${}^3\text{MC}$ ) on Ir(III) complex.

**3.2.1. Strong  $\sigma$  donor ligand: NHC (carbene complex).** N-Heterocyclic carbenes (NHCs) have attracted particular attention as ancillary ligands in catalysis because of their donating properties, steric hindrance, and stabilising properties.<sup>128,129</sup> These unique characteristics of NHCs have been applied in OLED research. In particular, NHCs can be easily tuned through imidazole-ring architecture modification, by changing the *N*-substituents or the backbone.<sup>130</sup> The carbene ligand has a stronger field than those of traditional N-heterocycle-based ligands; this increases the Ir–carbene bond strength and remarkably destabilises the LUMO levels. In addition, this strong Ir–carbene bond retards the  ${}^3\text{MC}$  state generation. Thus, the thermal- and photo-stabilities of these complexes are impressively high, as shown in Fig. 13. The first carbene-based Ir(III) complexes for blue OLEDs were reported by Thompson *et al.* in 2005.<sup>131</sup> Those researchers prepared new types of Ir(III) complex using high field-strength carbene ligands such as 1-phenyl-3-methylimidazolin-2-ylidene (pmi) and 1-phenyl-3-methylbenzimidazolin-2-ylidene (pmb), **65** and **66**, respectively, to destabilise the  ${}^3\text{MC}$  state. Hence, increments in the blue phosphorescent quantum yields were obtained. Crystal structure analysis showed that the average Ir–C<sub>carbene</sub> distance (2.026(7) Å) in **66** is significantly shorter than the average Ir–N distance in **63** (2.124(5) Å), which indicates that the carbene moiety is more strongly bound to the Ir than the pyrazolyl ligand. In addition, the lengthened distance of the average Ir–C<sub>phenyl</sub> bond in the carbene complexes exceeds the average Ir–C<sub>phenyl</sub> distance in **63**, confirming that the carbene is a stronger-field ligand than the pyrazolyl. Accordingly, strong-field carbene ligands destabilise thermally accessible non-emissive states, and carbene-based Ir(III) complexes exhibit higher PLQY than pyrazolyl-based complexes. In the same year, realisation of OLED devices with these complexes was reported by Forrest *et al.*, as a new development strategy for F-free blue phosphor.<sup>127</sup> Although the device EQE was low (5.8%), a deep-blue-emissive phosphorescent device with CIE coordination with (0.17, 0.06) was achieved.

Later, Da Como *et al.* prepared CN-substituted pmb-based Rh, Pt, and Ir carbene complexes to investigate the role of the SOC and  $\Delta E_{\text{ST}}$  in controlling the radiative phosphorescence

rate.<sup>132</sup> The CN-substituted Ir(III) complex, **67** (Fig. 14), exhibits enhanced PLQY up to 0.78, much higher than **66** (note that the PLQY of **66** was later corrected from 0.04 to 0.37).<sup>57</sup> This idea was extended to heteroleptic Ir(III) complexes with F-coordinated benzyl carbene main ligands and a 2-pyridyl triazolate ancillary ligand by Wu *et al.*, who reported complexes **68–70** (Fig. 14).<sup>133</sup> Those researchers observed significant blue-shifted emission through F-atom attachment, along with higher PLQY with insertion of a saturated methylene spacer in the main ligand. The enhanced PLQY was rationalised by estimating different NR decay rate constants for the reported complexes. Among the considered complexes, **70** was applied as a dopant in a blue OLED device. CIE coordinates of (0.158, 0.128) with an EQE of up to 6.0% were obtained. However, this value dropped to 2.7% at a practical brightness of 100 cd m<sup>-2</sup>. The results of a further theoretical investigation revealed remarkably destabilised HOMO energies through introduction of a methylene spacer in **69** and **70**; thus, the HOMO–LUMO energy gaps in these complexes were increased.<sup>134</sup>

Kido *et al.* reported another carbene complex, **71**, that exhibited blue emission with  $\lambda_{\text{max}}$  at 445 nm.<sup>135</sup> When **71** was doped with 3,6-bis(diphenylphosphoryl)-9-phenylcarbazole at 10 wt% (PO9, host) in film, high  $\eta_{\text{PL}}$  values of 0.70 were obtained with a  $\tau_{\text{p}}$  of 19.6  $\mu\text{s}$  at RT. This behaviour was compared with **1** and it was concluded that the strong ligand field effect in the carbene complex induces significant shifts in the d-orbital energies, which then facilitates high PLQY and longer lifetime. Additionally, **71** was combined with other red and green phosphors to fabricate a white OLED; the device exhibited  $\eta_{\text{p,max}}$  and  $\eta_{\text{p},1000}$  values of 59.9 and 43.3 lm W<sup>-1</sup>, respectively. Karatsu *et al.* systematically studied substitution effects on Ir(pmb)<sub>3</sub> (**66**) moieties, **72–75** (Fig. 14), using electron-donating ( $-\text{OCH}_3$ ) or withdrawing ( $-\text{CF}_3$  and  $-\text{CN}$ ) groups on the phenyl ring.<sup>136</sup> The luminescent properties were found to be greatly affected by the functional group on the phenyl moiety, whereas the geometries and electrochemical properties remained within a similar range.

In 2013, De Cola *et al.* first reported efficient deep-blue-emissive cationic bi-pincer Ir(III) carbene complexes, **76** and **77** (Fig. 14), which were obtained using a pincer-type ligand, (4,6-dimethyl-1,3-phenylene- $\kappa C^2$ )bis(1-butylimidazol-2-ylidene), with  $\text{I}^-$  and  $\text{PF}_6^-$  as counter anions.<sup>137</sup> Both complexes exhibit vibronic progression from the  ${}^3\text{LC}/{}^3\text{MLCT}$  excited states with two main emission maxima at 394 and 406 nm. The PLQYs of **76** and **77** in solution are higher than those of the other reported bis-tridentate Ir(III) complexes at 0.41 and 0.38, respectively, because of the presence of strong-field ligands and a more rigid tridentate system. Interesting features are found in the solid state. The crystals of **76** exhibit a large, dominant redshifted emission at 500 nm, whereas those of **77** exhibit dual emission with the original high-energy emission and an additional low-energy emission at approximately 500 nm. The effect of the counter anion is remarkably apparent in the amorphous film. At a 50% doping ratio, significant low-energy emission appears for **76**; however, **77** exhibits only

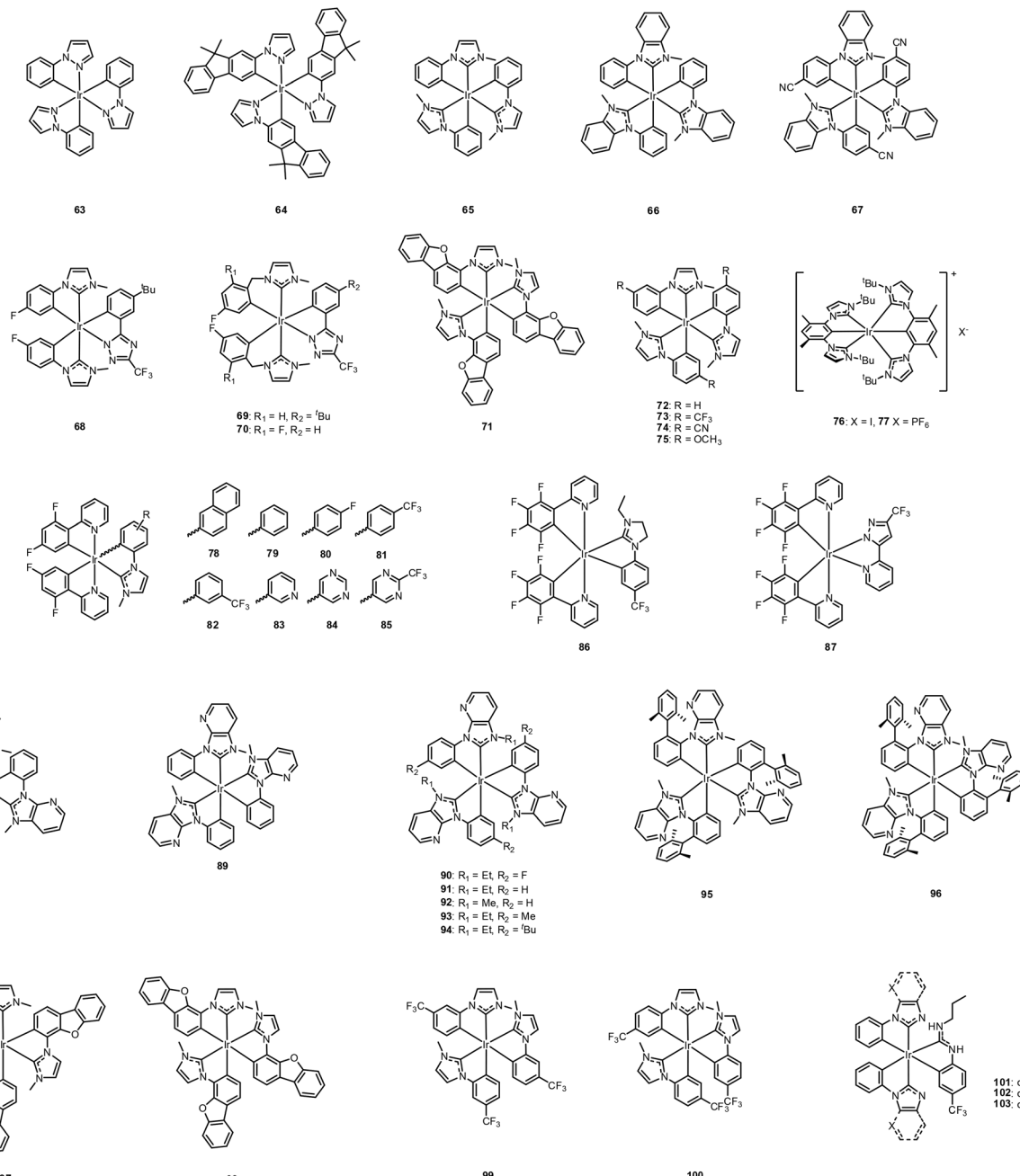


Fig. 14 Chemical structures of NHC-based carbene type Ir(III) complexes, 63–103.

a minor band in this region. Although the fabricated preliminary device exhibited very low efficiency (<1%), the EL spectrum showed saturated blue emission with maxima at 386 and 406 nm.

A series of N-heterocyclic carbene Ir(III) complexes, 78–85 (Fig. 14), having dfppy as the main ligand and NHCs as ancillary ligands, were systematically studied by Zuo *et al.* in 2015.<sup>138</sup> By modifying the phenyl moiety in the NHCs with electron-withdrawing substituents or replacing the phenyl ring with N-heteroaromatic rings, the HOMO–LUMO gaps were increased and the emissions were blue-shifted accordingly.

Among this series of carbene-based Ir(III) complexes, the 82-based blue phosphorescent OLED device exhibits good performance, with a maximum  $\eta_c$  of 37.83 cd A<sup>-1</sup>, an EQE of 10.3%, and an  $L_{max}$  of 8709 cd m<sup>-2</sup>. More recently, Wong *et al.*, reported heteroleptic iridium(III) complexes with NHC and acidic pyrazolyl-pyridine (fppz) moieties as ancillary ligands, 86 and 87, respectively.<sup>139</sup> These ancillary ligands successfully maintained the relatively high LUMO energy levels, because the LUMOs of these Ir(III) complexes are almost completely located on the antibonding  $\pi^*$  orbital of the pyridyl ring of the main ligand, F<sub>4</sub>ppy. Thus, sky-blue emissions at a wavelength

of around 465 nm with PLQYs of over 0.60. Accordingly, OLED devices were fabricated which afford high luminance values of over 10 000 cd m<sup>-2</sup> at a driving voltage of 10 V with peak current efficiencies of 47.6 and 45.5 cd A<sup>-1</sup>, corresponding to EQEs of 20.6% and 19.6% for **86**-based and **87**-based devices, respectively.

In 2016, impressive device efficiency enhancement using carbene-based Ir(III) complexes was reported by the Forrest group.<sup>140</sup> *N*-Phenyl, *N*-methylpyridoimidazole was used as a cyclometalating ligand and both *fac*- (**88**) and *mer*- (**89**) isomers of Ir(pmp)<sub>3</sub> were prepared (Fig. 14). Although their absorption and emission a slightly red-shifted compared to **66**, from 380 to 418 nm for **88** and to 465 nm for **89**, both complexes exhibit significantly higher PLQYs ( $\approx$ 0.77) compared to **66** (0.37).<sup>57</sup> This enhancement is due to the N atom in the pyridoimidazol-2-yl moiety, which modulates the LUMO energy level. As a result, the emissive triplet state is stabilised, and a concomitant increase is obtained in the energy gap between the emissive T<sub>1</sub> state and the non-emissive <sup>3</sup>MC state. Notably, both complexes show enhanced device performance. That is, the **88**-based device achieves a remarkable reduction in efficiency roll-off at high current density with high luminance (EQE = 10.1%), along with a deep-blue colour coordinate of (0.16, 0.09). The **89**-based device shows even higher efficiency with a high EQE of 14.4% and high luminance of  $>22\,000$  cd m<sup>-2</sup>. In particular, **88** can serve as the HTL and EBL material simultaneously. Available photophysical- and electrochemical data of **63–103** with their device performances are summarised in Table 4.

Zhou and Powell later calculated the possible reaction pathways of **88** and **66** to the NR <sup>3</sup>MC states, the correlation between the lowest activation barrier to the <sup>3</sup>MC states, and the experimental NR rate constants.<sup>141</sup> According to their calculations, the Ir–C bond of the NHC ligand is mostly elongated in the excited state for both isomers. In addition, those authors calculated the key parameters of the T<sub>1</sub> states: (1) the Franck–Condon state in the ground-state, (2) the optimised <sup>3</sup>MLCT state, (3) an intermediate <sup>3</sup>MC state, and (4) the optimised <sup>3</sup>MC state. When a benzannulated component of the NHC ligands is replaced with a fused pyridyl ring, transitioning from **66** to **88**, the energy barrier to the NR state is increased. Zhou and Powell explained that the presence of the N atom with greater electronegativity may strengthen the Ir–C (NHC) bond and generate a higher energy barrier in the <sup>3</sup>MC state, yielding a slower  $k_{nr}$  for **88**. More importantly, they found that the metal–ligand bond in the <sup>3</sup>MC state does not break away and is reversible. The PLQY enhancement of **88** may be due to this unique property.

In 2017, Wong *et al.* prepared a series of N-heterocyclic carbene Ir(III) complexes, **90–94**, to study the effect of electron-withdrawing/donating nature of the substituent on the phenyl ring by modifying **89**.<sup>142</sup> The device fabricated using **94** (Fig. 14) exhibited the maximum EQE, at 19.0% with restricted efficiency roll-off. Recently, Kang *et al.* modified the phenyl ring of **88** with a bulkier substituent, a xylyl ring at the *ortho* positions of pmb, to investigate the NR decay pathway accord-

ing to the ligand bulkiness.<sup>143</sup> The detailed photo-dynamics in the excited states were studied using transient absorption and time-resolved emission techniques in a series of Ir(III) complexes. When the bulkier ligand was attached, the PLQYs of both the *fac*- (**95**, Fig. 14) and *mer*- (**96**) isomers were anomalously quenched in the solution at 300 K. They found new, broad TA bands for **95** and **96** at approximately 720 nm with increasing delay time; this band was associated with structural changes in the excited triplet state which yielded fast localisation migration *via* inter-ligand charge transfer and influenced the deactivation pathway to quench the emission intensity.

*N*-Dibenzofuranyl-*N*-methylimidazole-based Ir(III) carbene complexes with *fac*- (**97**) and *mer*- (**98**, Fig. 14) isomers was also reported by our group.<sup>144</sup> For the previously reported Ir(III) carbene complexes, the *mer*-isomer is equally or more efficiently luminescent than the *fac*-isomer in solution and in the solid state,<sup>131,140</sup> however, the *fac*-isomer labelled **97** exhibits better luminescence properties in solution and device application than the *mer*-isomer labelled **98**. We rationalised this difference using DFT calculations, which revealed that the energy barrier from T<sub>1</sub> to <sup>3</sup>MC of **98** is lower than that of **97**. Among the two OLED devices, the **97**-based device showed a higher EQE value (18.5%) than the **98**-based device (18.2%). Furthermore, the CIE<sub>x,y</sub> for the **97**-based device showed a deeper blue coordination of (0.14, 0.11) compared to the **98**-based device with (0.14, 0.14).

Zysman-Colman *et al.* reported two kinds of –CF<sub>3</sub> functionalised *mer*-Ir(pmi)<sub>3</sub> complexes, **99** and **100** (Fig. 14), in which the substitution position of –CF<sub>3</sub> on the phenyl ring was varied to obtain a high PLQY through sufficient stabilisation of the HOMO energy level.<sup>121</sup> Both complexes show structured deep-blue emission ( $\lambda_{max} \approx 425$  nm) in degassed dichloromethane at RT. However, the PLQYs are significantly affected depending on the substitution position. For **99**, the PLQY is relatively low at 0.25, whereas that of **100** is considerably higher at 0.72, being comparable to **89**. An optimised device with **100** as a blue dopant and **99** as an efficient exciton/electron blocker exhibited deep-blue CIE coordinates of (0.154, 0.052), with an EQE<sub>max</sub> of 13.4% and an EQE of 12.5% at 100 cd m<sup>-2</sup>.

Most recently, Teets *et al.* reported a new type of Ir(III) carbene complex with an acyclic diaminocarbene (ADC) as an ancillary ligand, **101–103** (Fig. 14), referred to as a ‘mixed-carbene complex’.<sup>145</sup> These mixed-complexes were prepared through a cascade reaction with nucleophilic addition reaction followed by base-assisted cyclometalation reaction of the ADC intermediate. Compared to homoleptic Ir(III) carbene complexes, the mixed-carbene complexes show the same or even better photoluminescence characteristics; for example, higher PLQY. As ADC is an even stronger  $\sigma$ -donor ligand than NHCs, because of its greater 2p in its s orbital, the molecular design strategy for saturated blue emissive material may be extended following this approach.

### 3.3. Rigid structure for restricted intramolecular motion

Increments of PLQY are often observed for cyclometalated Ir(III) complexes in solid states, such as frozen solutions and

Table 4 Available photophysical- and electrochemical data of 63–103 with their device performances

Photophysical properties					Device performances					Ref.
$\lambda_{\text{em}}$ (nm)	$\tau_{\text{em}}$ (μs)	PLQY	$k_r$ (s <sup>-1</sup> )	$k_{\text{nr}}$ (s <sup>-1</sup> )	Oxidation (V)	EL ( $\lambda_{\text{max}}$ , nm)	CIE (x, y)	EQE <sub>max</sub> (%)	Ref.	
63	414 <sup>a</sup>	14.0	—	—	0.41	—	—	—	—	131
64	480	37.0	0.38	$0.1 \times 10^5$	$0.2 \times 10^5$	0.31	—	—	—	131
65	380 <sup>a</sup>	0.4	0.02	$0.5 \times 10^5$	$2.0 \times 10^6$	0.22	—	—	—	131
66	389	0.22	0.04	$1.8 \times 10^5$	$4.3 \times 10^6$	—	—	—	—	131
67	380	—	0.78	$4.9 \times 10^4$	$1.3 \times 10^4$	—	—	—	—	132
68	392, 461	0.001	<0.001	$6.0 \times 10^5$	$1.2 \times 10^9$	—	—	—	—	133
69	460	0.22	0.22	$1.0 \times 10^6$	$3.5 \times 10^6$	—	—	—	—	133
70	458	0.38	0.73	$1.9 \times 10^6$	$7.0 \times 10^5$	—	434, 460	(0.16, 0.13)	6.0	133
71	445	19.6 <sup>b</sup>	0.70 <sup>b</sup>	$0.4 \times 10^6$	$0.2 \times 10^5$	—	—	—	—	135
72	390, 407	1.3	0.44	$3.4 \times 10^{-5}$	$4.3 \times 10^{-5}$	0.45	—	—	—	136
73	396, 416	6.1	0.84	$1.4 \times 10^{-5}$	$0.3 \times 10^{-5}$	0.74	—	—	—	136
74	521, 445	14.0	0.71	$0.5 \times 10^{-5}$	$0.2 \times 10^{-5}$	0.84	—	—	—	136
75	403, 415	5.0	0.76	$1.5 \times 10^{-5}$	$0.5 \times 10^{-5}$	0037	—	—	—	136
76	384, 406	8.9	0.41	$4.6 \times 10^{-5}$	$6.6 \times 10^{-5}$	0.68	—	—	—	137
77	384, 406	9.4	0.38	$4.1 \times 10^{-5}$	$6.5 \times 10^{-5}$	0.65	386, 406	—	—	137
78	483	2.1	0.14	$0.6 \times 10^5$	$3.7 \times 10^5$	—	—	—	—	138
79	483	1.8	0.65	$3.6 \times 10^5$	$1.9 \times 10^5$	—	—	—	—	138
80	473	1.8	0.73	$4.1 \times 10^5$	$1.5 \times 10^5$	—	—	—	—	138
81	469	1.9	0.57	$3.0 \times 10^5$	$0.2 \times 10^5$	—	—	—	—	138
82	469	1.8	0.69	$3.8 \times 10^5$	$1.7 \times 10^5$	—	470	—	10.3	138
83	473, 498	1.8	0.61	$3.4 \times 10^5$	$2.2 \times 10^5$	—	—	—	—	138
84	471, 497	1.7	0.33	$1.9 \times 10^5$	$3.9 \times 10^5$	—	—	—	—	138
85	455, 479	1.9	0.32	$1.7 \times 10^5$	$3.6 \times 10^5$	—	—	—	—	138
86	469, 462	17.6	0.60	$0.3 \times 10^5$	$0.2 \times 10^5$	—	465	(0.19, 0.39)	20.6	139
87	462, 459	16.6	0.68	$0.4 \times 10^5$	$0.2 \times 10^5$	—	—	(0.19, 0.37)	19.6	139
88	418	1.2	0.76	$6.4 \times 10^5$	$2.0 \times 10^5$	0.23	—	—	—	140
89	465	0.8	0.78	$1.0 \times 10^6$	$2.7 \times 10^5$	—	—	—	—	140
90	430	3.8	0.98	$2.6 \times 10^5$	$0.5 \times 10^4$	—	—	—	—	142
91	454	4.5	0.85	$1.9 \times 10^5$	$0.3 \times 10^5$	—	—	(0.15, 0.19)	7.6	142
92	468	4.3	0.99	$2.3 \times 10^5$	$0.2 \times 10^4$	—	—	(0.15, 0.19)	10.8	142
93	469	4.7	0.45	$1.0 \times 10^5$	$1.2 \times 10^5$	—	450	(0.15, 0.19)	15.2	142
94	422	5.3	0.33	$0.6 \times 10^5$	$1.2 \times 10^5$	—	—	—	—	142
95	515	0.17	0.03	$1.8 \times 10^5$	$5.9 \times 10^6$	0.43	—	—	—	143
96	555	0.0037	0.001	$2.7 \times 10^5$	$2.7 \times 10^8$	0.29	—	—	—	143
97	444, 472	11.2	0.68	$6.1 \times 10^4$	$2.9 \times 10^4$	—	—	(0.14, 0.11)	18.5	144
98	450, 477	11.0	0.53	$4.8 \times 10^4$	$4.1 \times 10^4$	—	—	(0.14, 0.14)	18.2	144
99	414, 424	0.3, 1.8	0.25	—	—	0.88	—	—	—	121
100	412, 427	0.7, 1.8	0.72	—	—	0.80	431	(0.15, 0.08)	7.2	121
101	418 <sup>b</sup>	6.1 <sup>b</sup>	0.13 <sup>b</sup>	$0.2 \times 10^{-5}$	$1.4 \times 10^{-5}$	0.16	—	—	—	145
102	418 <sup>b</sup>	1.8 <sup>b</sup>	0.31 <sup>b</sup>	$1.7 \times 10^{-5}$	$3.8 \times 10^{-5}$	0.21	—	—	—	145
103	459 <sup>b</sup>	0.9 <sup>b</sup>	0.48 <sup>b</sup>	$5.6 \times 10^{-5}$	$6.1 \times 10^{-5}$	0.25	—	—	—	145

<sup>a</sup> Measured at 77 K. <sup>b</sup> Doped film.

doped polymer films. For example, Chou *et al.* found that the solid-state PLQY can be increased by more than one order compared to that in solution.<sup>146</sup> This result suggests that an cyclometalated Ir(III) complex with rigid conformation that can suppress motional relaxations may yield increased PLQY. (The structural origin of these behaviours can be understood by considering the temperature-independent decay process (vibronic-coupled NR decay process) described above.) Therefore, cyclometalated Ir(III) complexes with rigid structures have been extensively studied for restriction of intramolecular motions to minimise the NR decay process.

**3.3.1. Bis-tridentate Ir(III) complexes.** Use of a bis-tridentate rather than a tris-bisidentate ligand may be a natural means of inducing molecular rigidity. Ir(III) bis-terpyridine,  $[\text{Ir}(\text{tpy})_2]^{3+}$  (104, Fig. 15), which may be the first such example,

was previously reported by DeGraff *et al.* and exhibited greenish blue emission upon excitation in the near-UV.<sup>147,148</sup> The Williams group extended the synthetic method and luminescence properties of bis-tridentate Ir(III) complexes.<sup>149–151</sup> For example, they reported the first instance of a charge-neutral cyclometalated Ir(III) complex containing two terdentate ligands, binding *via*  $N^{\wedge}C^{\wedge}N$  and  $C^{\wedge}N^{\wedge}C$  coordination modes and here labelled 105 and 106 (Fig. 15).<sup>152</sup> However, the emission is at approximately 585 nm for those complexes. Haga *et al.* also reported bis-tridentate Ir(III) complexes based on benzimidazole ligands, 107–110 (Fig. 15).<sup>153</sup> The  $^3\text{MLCT}$  contribution in the excited state is dependent on the  $\sigma$ -donating ability of the tridentate ligand, which affects the radiative rate. However, these complexes also emit in a range far from the saturated blue colour. In addition, the photoluminescence efficiency is generally lower than those of tris-bidentate Ir(III)

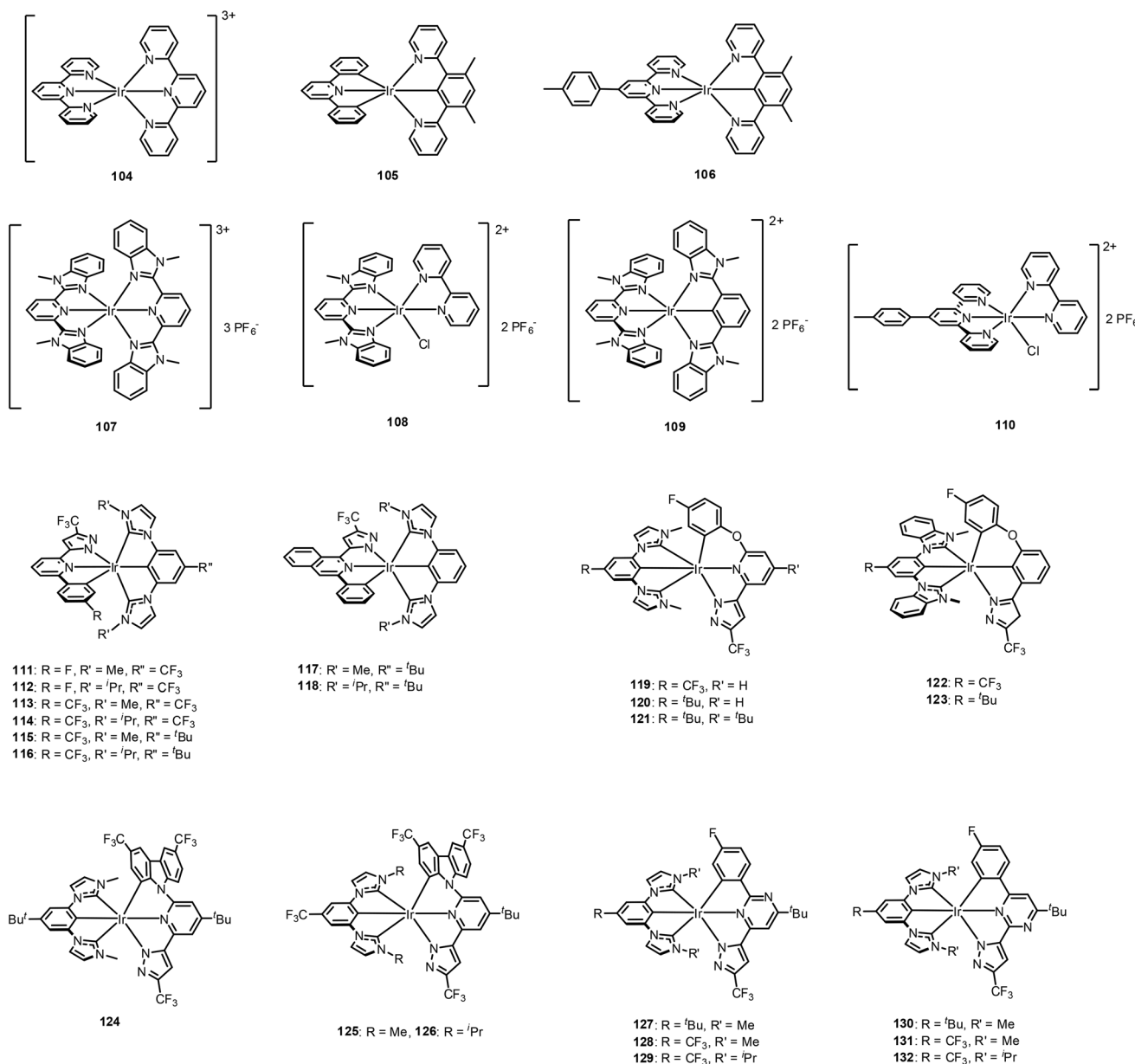


Fig. 15 Chemical structures of bis-tridentate  $\text{Ir}(\text{III})$  complexes, 104–132.

complexes because of the weaker ligand-field strengths originating from the poorer bite angles.<sup>154</sup>

Following the above works, extensive studies were subsequently performed to develop a blue-emissive bis-tridentate  $\text{Ir}(\text{III})$  complex. In 2016, the Chi group reported cooperation between bis(imidazolylidene) benzenes and functionalised 2-pyrazolyl-6-phenyl pyridine (or isoquinoline) chelates ligands to form bis-tridentated  $\text{Ir}(\text{III})$  complexes, 111–118 (Fig. 15).<sup>155</sup> Although the most blue-shifted emission among this series is at 467 nm for solution 111, the methyl-substituted complexes exhibit almost unitary PLQY whereas the isopropyl-substituted complexes exhibit lower PLQY. This difference was rationalised by considering the reduction in the torsional vibration degrees of freedom for the methyl groups. The researchers also noted

that increases in the rigidity and multidentate coordination mode are key factors yielding the excellent PL and EL efficiency obtained for these complexes. Depending on the  $\pi$ -conjugation and/or electronic characteristics of the chelates, the emission colour can be finely tuned. Accordingly, the authors successfully fabricated efficient, independent red, green, and blue OLED devices. They also obtained a white OLED device by combining these dopants in the emitting layer. For example, 95% doping in a 9-(3-(9*H*-carbazol-9-yl) phenyl)-9*H*-carbazole-3-carbonitrile (mCPCN) host yielded blue-emitting OLEDs with an EQE of 27% and  $\text{CIE}_{x,y}$  of (0.18, 0.40). To enlarge the HOMO–LUMO energy band gap of this sky-blue dopant, the same group designed new  $\text{Ir}(\text{III})$  complexes in which the 6-pyrazolyl-2-ppy was replaced with 6-pyra-

Table 5 Available photophysical- and electrochemical data of 104–132 with their device performances

Photophysical properties					Device performances					
	$\lambda_{\text{em}}$ (nm)	$\tau_{\text{em}}$ (μs)	PLQY	$k_r$ (s <sup>-1</sup> )	$k_{\text{nr}}$ (s <sup>-1</sup> )	Oxidation (V)	EL ( $\lambda_{\text{max}}$ , nm)	CIE ( $x, y$ )	EQE <sub>max</sub> (%)	Ref.
104	506	9.5	0.11	$0.1 \times 10^5$	$1.0 \times 10^5$	>1.7	—	—	—	153
105	585	3.9	0.21	$3.4 \times 10^5$	$1.2 \times 10^6$	—	—	—	—	152
106	560	—	—	—	—	—	—	—	—	152
107	550, 592	1.0	0.04	$0.4 \times 10^5$	$8.9 \times 10^6$	1.65	—	—	—	153
108	547, 582	5.7	0.19	$0.3 \times 10^5$	$1.4 \times 10^6$	1.64	—	—	—	153
109	593, 623	1.6	0.10	$0.6 \times 10^5$	$5.7 \times 10^5$	1.18	—	—	—	153
110	509, 541	1.2	0.04	$0.4 \times 10^5$	$9.1 \times 10^5$	>1.7	—	—	—	153
111	467, 501	5.4	0.99	$1.8 \times 10^5$	$0.1 \times 10^4$	—	—	(0.18, 0.40)	27.0	155
112	468, 503	6.7	0.86	$1.3 \times 10^5$	$0.2 \times 10^5$	—	—	(0.19, 0.39)	20.8	155
113	490, 526	4.7	0.92	$2.0 \times 10^5$	$0.2 \times 10^5$	—	—	(0.29, 0.57)	30.0	155
114	492, 529	4.4	0.80	$1.8 \times 10^5$	$0.5 \times 10^5$	—	—	(0.28, 0.57)	28.3	155
115	501, 535	2.8	1.00	$3.6 \times 10^5$	—	—	—	(0.34, 0.60)	31.4	155
116	503, 537	3.0	0.98	$3.3 \times 10^5$	$0.7 \times 10^4$	—	—	(0.34, 0.60)	30.0	155
117	593, 643	8.2	1.00	$1.2 \times 10^5$	—	—	—	(0.63, 0.38)	27.4	155
118	595, 647	6.9	0.98	$1.4 \times 10^5$	$0.3 \times 10^4$	—	—	(0.63, 0.38)	20.0	155
119	471	25.1	0.81	$0.3 \times 10^5$	$0.7 \times 10^4$	0.67	—	—	—	156
120	478	4.42	0.82	$1.9 \times 10^5$	$0.4 \times 10^5$	0.53	—	(0.15, 0.24)	19.7	156
121	472	8.66	0.72	$0.8 \times 10^5$	$0.3 \times 10^5$	0.52	—	(0.15, 0.17)	20.7	156
122	473	61.2	0.68	$0.1 \times 10^5$	$0.5 \times 10^4$	0.80	—	—	—	156
123	473	18.6	0.79	$0.4 \times 10^5$	$0.1 \times 10^5$	0.62	—	—	—	156
124	486	2.8	1.00	$3.6 \times 10^5$	—	0.55	484	(0.19, 0.34)	19.6	157
125	473	3.2	0.84	$2.6 \times 10^5$	$0.5 \times 10^5$	0.69	468	(0.17, 0.25)	21.6	157
126	476	2.7	0.83	$3.1 \times 10^5$	$0.6 \times 10^5$	0.68	472	(0.17, 0.26)	19.6	157
127	506	2.59	0.92	$7.7 \times 10^{-5}$	—	0.48	—	—	—	158
128	489	4.43	0.94	$8.2 \times 10^{-5}$	—	0.75	—	—	—	158
129	491	3.89	1.00	$9.2 \times 10^{-5}$	—	0.59	—	—	—	158
130	515	0.93	0.96	$2.8 \times 10^{-5}$	—	0.37	—	—	—	158
131	473	1.52	0.97	$3.3 \times 10^{-5}$	—	0.67	—	—	—	158
132	477	1.53	1.00	$3.7 \times 10^{-5}$	—	0.62	—	—	—	158

zolyl-2-phenoxyppyridine to break the  $\pi$ -conjugation between the pyridyl and fluorophenyl units.<sup>156</sup> As expected, all emission spectra of these 6-pyrazolyl-2-phenoxyppyridine based complexes, 119–121 (Fig. 15), are clearly blue-shifted *versus* the emission spectra for the 6-pyrazolyl-2-ppy-based Ir(III) complexes, 111–116 (Fig. 15). Note that deep-blue EL with an EQE of >20% and CIE<sub>x,y</sub> = (0.15, 0.17) were achieved using 121 as a dopant material. Available photophysical- and electrochemical data of 104–132 with their device performances are summarised in Table 5.

Next, the Chi group employed a carbazolyl unit to replace the phenoxy group.<sup>157</sup> The resultant carbazole-based Ir(III) complexes, 124–126 (Fig. 15), exhibit structureless emission bands indicating the dominant charge transfer contribution in the emissive process, with maxima at 486, 473, and 476 nm, respectively. The PLQY is almost unitary for 124, and slightly lower, at approximately 83%, for both 125 and 126 in solution at RT. Surprisingly, the radiative lifetimes ( $\tau_{\text{rad}}$ ) of 124–126 are significantly shorter (2.77–3.80 μs) than those of the previously reported Ir(III) complexes, 111 and 121, ( $\tau_{\text{rad}} = 5.41$  and 12.0 μs). This may be advantageous for application of these materials in device structures, because it may reduce the population density of the long-lived triplet excitons. Importantly, the Chi group also conducted photo-degradation experiments on the complexes in deaerated toluene under irradiation. The carbazole-based bis-tridentate Ir(III) complexes exhibits superior photostability to the tri-bisdentate deep-blue Ir(III)

carbene complexes, 88 and 89. Furthermore, the rate of photo-degradation of the carbazole-based Ir(III) complexes is lower than those of 111 and 121, indicating that the six-membered *N*-containing metallacycle in these complexes is more stable than the corresponding five-membered metallacycle system as a result of the robust chelating framework. More recently, improved photo-stabilities with shortened  $\tau_{\text{em}}$  were obtained by replacing the central pyridine unit with a pyrimidine unit, 127–132 (Fig. 15).<sup>158</sup> Various methodologies for fine-tuning the electronic transitions of bis-tridentate Ir(III) complexes for high performance and durable phosphorescent OLEDs are being developed at present.<sup>159–162</sup>

**3.3.2. Bridged diiridium complexes.** In contrast to the developments pertaining to mononuclear cyclometalated Ir(III) complexes, the fundamental chemistry and OLED applications of diiridium complexes are under-researched because of their relatively large molecular weights and lower PLQYs.<sup>163–167</sup> Moreover, diiridium complexes are often obtained as a mixture of diastereomers.<sup>168</sup> However, diiridium systems also have important advantages such as increased spin-orbit coupling due to the presence of multiple metal centres, higher stability due to the improved chelating effect of the bridging ligand, and the possibility of intramolecular  $\pi$ – $\pi$  interactions, which can induce a rigid conformation and reduce  $k_{\text{nr}}$ .<sup>168</sup> Recent prudent choices of bridging ligand have clearly shown that inferior optical properties are inevitable; this is well-documented in relevant review articles.<sup>169,170</sup> The main challenge

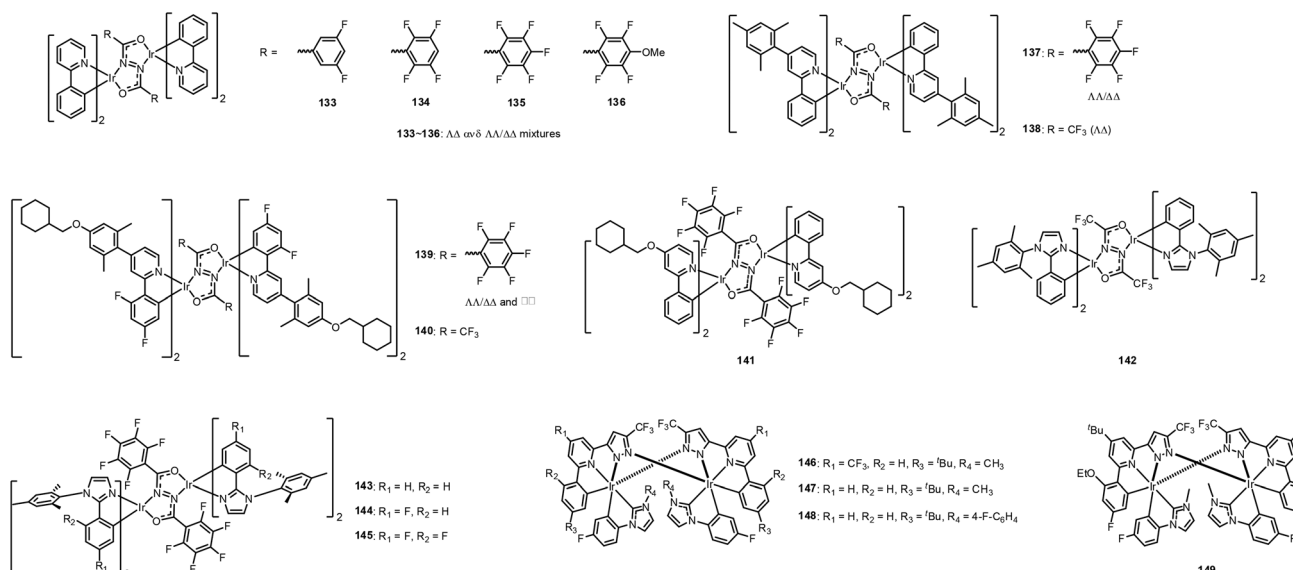


Fig. 16 Chemical structures of diiridium complexes, 133–149.

concerning diiridium complexes is achievement of efficient and stable blue electroluminescence. Indeed, blue-emitting diiridium complexes have rarely been reported.

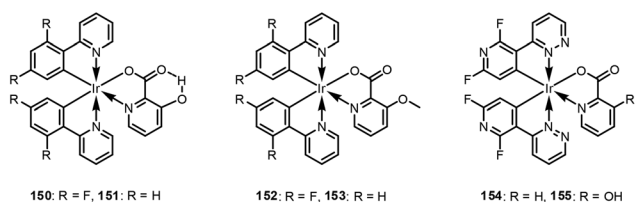
Recently, Bryce *et al.*, reported a series of diarylhydrazide-bridged diiridium complexes functionalised withppy-based cyclometalating ligands, 133–141 (Fig. 16).<sup>171</sup> Among them, 141 exhibits sky-blue emission in doped film with  $\lambda_{\text{max}} = 460$  nm; this value indicates 10 nm hypsochromic shifting compared to 1. This complex also exhibits high PLQY (0.69), high  $k_r$  ( $4.26 \times 10^5 \text{ s}^{-1}$ ), and relatively short  $\tau_p$  (2.24  $\mu\text{s}$ ) in doped film. A combination of X-ray molecular structure analyses and NMR studies have revealed that the intramolecular  $\pi$ – $\pi$  interactions between the bridging and cyclometalating ligands rigidify the complexes and play an important role in the observed, excellent photophysical properties. Bryce *et al.* continued their work using hydrazide-bridged diiridium complexes, 142–145 (Fig. 16).<sup>172</sup> Complexes 143–145 are strongly emissive (PLQYs = 0.47–0.55) when doped into PMMA, whereas complex 142 exhibits a relatively small PLQY of 0.11. Those researchers interpreted these findings as indicating that the intramolecular  $\pi$ – $\pi$  interactions are promoted by introduction of F substituents to the phenyl rings of the bridging ligand. In 2018, Chi *et al.* reported sublimable diiridium complexes bearing both functional 2-pyrazolyl-6-phenyl pyridine chelate and bidentate phenyl imidazolylidene chelate, 146–149 (Fig. 16).<sup>173</sup> Among them, 149 exhibits blue-shifted emission peaks at 468, 500, and 536 nm due to the combined inductive and mesomeric effects. Importantly, very high PLQYs of >0.90 were observed for all diiridium complexes in both solution and film states at RT. Accordingly, the resulting OLED device using 149 showed impressive blue-emitting characteristics with an EQE of 14.2%. It should be noted OLED devices with 146 and 147 showed much higher EQEs of 18.3% (yellowish green colour) and 27.6% (green colour), respectively. These

investigations of diiridium complexes offer a new method for future development of deeper-blue emitting Ir(III) complexes. Available photophysical- and electrochemical data of 133–149 with their device performances are summarised in Table 6.

**3.3.3. Intramolecular hydrogen bond for restricting intramolecular motion in the excited state.** Our group reported the following alternative approach to improving the stability of blue phosphorescent dopant material.<sup>174</sup> As the deactivation process is induced by the formation of five-coordinated trigonal bipyramidal species through dissociation of the Ir–N bond in the  $^3\text{MC}$  excited state, stability enhancement is expected if the trigonal bipyramidal geometry formation is disturbed by increasing the ancillary ligand rigidity (which can limit the degrees of freedom). In this regard, the ancillary ligand of 2 was modified by attaching the hydroxyl group at the 3-position of the picolinic acid; hence, 150 was obtained (Fig. 17). For comparison, a methoxy-substituted Ir(III) complex, 152, was also prepared. In the crystal structure of the non-fluorinated Ir(III) complex, 151 (Fig. 17), an intramolecular OH...O=C H bond involving phenolic OH and a non-bonded carboxylate O atom was confirmed. Attachment of the hydroxyl group does not affect the steady state photophysical properties. Note that 150 shows similar emission behaviour to 2, with emission maxima at 468 and 494 nm and a PLQY of 0.94. However, the rigid structure of 150 induced by the intramolecular hydrogen bond significantly affects the excited-state kinetics. The  $\tau_{\text{em}}$  of 150 is substantially longer than those of either 151 or 2 at both 300 and 77 K. The role of the intramolecular hydrogen bond in the excited state of 150 was confirmed by comparing the lifetimes in dichloromethane (DCM) solution and DMSO solution, where the latter can prevent the intramolecular hydrogen bond but induce the intermolecular hydrogen bond. The  $\tau_{\text{em}}$  of 150 in DMSO solution (2.13  $\mu\text{s}$ ) is significantly shorter than that measured in DCM solution (3.19  $\mu\text{s}$ ). These results clearly indi-

**Table 6** Available photophysical- and electrochemical data of 133–149 with their device performances

	Photophysical properties					Device performances				Ref.
	$\lambda_{\text{em}}^{\text{em}}$ (nm)	$\tau_{\text{em}}$ (μs)	PLQY	$k_{\text{r}}$ (s <sup>-1</sup> )	$k_{\text{nr}}$ (s <sup>-1</sup> )	Oxidation (V)	EL ( $\lambda_{\text{max}}$ , nm)	CIE (x, y)	EQE <sub>max</sub> (%)	
133	516 <sup>a</sup>	1.8 <sup>a</sup>	0.61 <sup>a</sup>	$3.4 \times 10^5$	$2.2 \times 10^5$	0.42, 0.67	—	—	—	171
134	503 <sup>a</sup>	2.0 <sup>a</sup>	0.59 <sup>a</sup>	$3.0 \times 10^5$	$2.1 \times 10^5$	0.52, 0.77	—	—	—	171
135	503 <sup>a</sup>	2.1 <sup>a</sup>	0.71 <sup>a</sup>	$3.4 \times 10^5$	$1.4 \times 10^5$	0.56, 0.81	—	—	—	171
136	507 <sup>a</sup>	2.0 <sup>a</sup>	0.66 <sup>a</sup>	$3.3 \times 10^5$	$1.7 \times 10^5$	0.50, 0.76	—	—	—	171
137	507 <sup>a</sup>	11.4 <sup>a</sup>	0.72 <sup>a</sup>	$5.2 \times 10^5$	$2.0 \times 10^5$	0.58, 0.90	—	—	—	171
138	504 <sup>a</sup>	1.1 <sup>a</sup>	0.66 <sup>a</sup>	$5.8 \times 10^5$	$3.0 \times 10^6$	0.62, 0.78	—	—	—	171
139	470	1.2	0.65 <sup>a</sup>	$5.5 \times 10^5$	$3.0 \times 10^5$	0.93, 1.28	—	—	—	171
	472 <sup>a</sup>	1.2 <sup>a</sup>	0.60 <sup>a</sup>	$5.5 \times 10^5$	$3.4 \times 10^5$	0.97, 1.33	—	—	—	171
140	471 <sup>a</sup>	1.1 <sup>a</sup>	0.46 <sup>a</sup>	$4.1 \times 10^5$	$4.8 \times 10^5$	0.95, 1.12	—	—	—	171
141	460 <sup>a</sup>	1.6 <sup>a</sup>	0.69 <sup>a</sup>	$4.3 \times 10^5$	$2.0 \times 10^5$	0.81, 1.18	—	—	—	171
142	500 <sup>a</sup>	1.8 <sup>a</sup>	0.11 <sup>a</sup>	$0.6 \times 10^5$	$4.9 \times 10^5$	0.34, 0.60	—	—	—	172
143	501 <sup>a</sup>	2.8 <sup>a</sup>	0.55 <sup>a</sup>	$2.0 \times 10^5$	$1.6 \times 10^5$	0.30, 0.67	—	—	—	172
144	486 <sup>a</sup>	4.2 <sup>a</sup>	0.47 <sup>a</sup>	$1.1 \times 10^5$	$1.3 \times 10^5$	0.49, 0.89	—	—	—	172
145	480 <sup>a</sup>	4.6 <sup>a</sup>	0.52 <sup>a</sup>	$1.1 \times 10^5$	$1.1 \times 10^5$	0.68, 1.12	—	—	—	172
146	531	3.0	0.98	$3.3 \times 10^5$	$0.1 \times 10^5$	0.64, 0.94	530	0.36, 0.61	18.3	173
147	487, 521, 559	4.6	0.95	$2.1 \times 10^5$	$0.1 \times 10^5$	0.50, 0.78	489	0.19, 0.53	27.6	173
148	485, 519, 554	7.0	0.64	$0.9 \times 10^5$	$0.5 \times 10^5$	0.58, 0.89	—	—	—	173
149	531	2.9	0.91	$3.1 \times 10^5$	$0.3 \times 10^5$	0.61, 0.92	—	—	—	173

<sup>a</sup> Doped film.**Fig. 17** Ir(III) complexes for investigating effects of intramolecular hydrogen bond.

cate that the intramolecular hydrogen bond in the ancillary ligand maintains the constrained geometry in the excited state and affords stable blue phosphorescence, facilitating fast radiative emission and retarding NR emission processes. The effect of an intramolecular hydrogen bond in real applications was evaluated for two OLED devices fabricated using 150 and 2 as dopant materials. The 150- and 2-based devices exhibited similar efficiencies, with EQEs of 18.1 and 19.0%, respectively. However, the

device operation lifetime was significantly improved for the 150-based device compared to 2-based device. Zhang *et al.* theoretically investigated this strategy using heteroleptic Ir(III) complexes with 3-(2,6-difluoropyridin-3-yl)pyridazine as a main ligand and picolinic acid 154 or 3-hydroxypicolinic acid 155 as an ancillary ligand (Fig. 17).<sup>175</sup> They performed independent calculations for this complex with and without an intramolecular hydrogen bond, to confirm the influence of the hydrogen bond on the PLQY. According to their calculations, 155 has a larger quantum yield than the other two complexes, which is mainly attributed to it having the smallest temperature-dependent  $k_{\text{nr}}(T)$ . The potential energy profiles of the deactivation pathway from the  $^3\text{MLCT}/\pi-\pi^*$  state to the  $S_0$  state *via* the  $^3\text{MC}_{\text{d-d}}$  state for 154 and 155 suggest that  $^3\text{MC}_{\text{d-d}}$  state formation is most difficult for 155, because of the rigid environment induced by the intramolecular hydrogen bond. Both studies clearly indicate that formation of an intramolecular hydrogen bond constitutes a new method for the design of new phosphors with the desired properties. Available photophysical- and electrochemical data of 150–155 with their device performances are summarised in Table 7.

**Table 7** Available photophysical- and electrochemical data of 150–155 with their device performances

	Photophysical properties					Device performances				Ref.
	$\lambda_{\text{em}}$ (nm)	$\tau_{\text{em}}$ (μs)	PLQY	$k_{\text{r}}$ (s <sup>-1</sup> )	$k_{\text{nr}}$ (s <sup>-1</sup> )	Oxidation (V)	EL ( $\lambda_{\text{max}}$ , nm)	CIE (x, y)	EQE <sub>max</sub> (%)	
150	468, 494	3.2	0.94	$3.0 \times 10^{-5}$	$0.3 \times 10^{-5}$	—	—	(0.15, 0.35)	18.1	174
151	501, 526	0.2	0.20	$9.1 \times 10^{-5}$	$3.6 \times 10^{-4}$	—	—	—	—	174
152	469, 495	0.9	0.72	$7.7 \times 10^{-5}$	$3.0 \times 10^{-5}$	—	—	—	—	174
153	506, 529	0.2	0.15	$9.4 \times 10^5$	$5.3 \times 10^{-4}$	—	—	—	—	174
154	472	14.9	0.70	$4.7 \times 10^4$	$2.0 \times 10^4$	—	—	—	—	175
155	533	18.3	0.77	$4.2 \times 10^4$	$1.3 \times 10^4$	—	—	—	—	175

## 4. Conclusions

Phosphorescent cyclometalated Ir(III) complexes are currently being used as key materials in highly efficient OLEDs, because of the high quantum efficiency and colour tunability, which are attributed to the various synthetic protocols and which afford functionalisation diversity. However, exploration of efficient blue phosphorescent Ir(III) complexes remains a challenge because of their relatively inadequate CIE coordinates and low PLQY efficiency. In this review, we summarised the fundamental photophysics and design strategies of blue phosphorescent Ir(III) complexes, including recent progress. Experimental and theoretical studies have shown that the HOMO and LUMO energy levels can be controlled by substituting electron-withdrawing groups into cyclometalate ligands and replacing phenyl rings with N-heteroaromatic rings, respectively. To suppress the NR decay processes in the excited states of cyclometalate Ir(III) complexes, two mechanisms should be considered: the vibronic-coupled NR decay process and crossing from the emissive state to an upper non-emissive  $^3\text{MC}$  excited state. This review surveyed several strategies towards development of efficient blue phosphorescent Ir(III) complexes, including the effects of a rigid structure providing restricted intramolecular motion and utilisation of ligands with strong  $\sigma$  donation ability to destabilise the  $^3\text{MC}$  state. Based on the strategies described herein, further improvements regarding the colour purity and phosphorescent efficiency of Ir(III) complexes can be expected, through design of smart ligands that can control the molecular geometry and electronic perturbation. We hope that this review will provide helpful guidance for future researchers towards the development of highly efficient blue phosphorescent Ir(III) complexes.

## Conflicts of interest

There are no conflicts to declare.

## Acknowledgements

This work was supported by the National Research Foundation of Korea (2019R1F1A1058578).

## References

- 1 M. A. Baldo, D. F. O'Brien, Y. You, A. Shoustikov, S. Sibley, M. E. Thompson and S. R. Forrest, Highly efficient phosphorescent emission from organic electroluminescent devices, *Nature*, 1998, **395**, 151–154.
- 2 M. A. Baldo, M. E. Thompson and S. R. Forrest, High-efficiency fluorescent organic light-emitting devices using a phosphorescent sensitizer, *Nature*, 2000, **403**, 750–753.
- 3 Y. You and W. Nam, Photofunctional triplet excited states of cyclometalated Ir(III) complexes: beyond electroluminescence, *Chem. Soc. Rev.*, 2012, **41**, 7061–7084.
- 4 M. A. Baldo, S. Lamansky, P. E. Burrows, M. E. Thompson and S. R. Forrest, Very high-efficiency green organic light-emitting devices based on electrophosphorescence, *Appl. Phys. Lett.*, 1999, **75**, 4–6.
- 5 C. Adachi, M. A. Baldo, S. R. Forrest and M. E. Thompson, High-efficiency organic electrophosphorescent devices with tris(2-phenylpyridine)iridium doped into electron-transporting materials, *Appl. Phys. Lett.*, 2000, **77**, 904–906.
- 6 B. W. D'Andrade, M. A. Baldo, C. Adachi, J. Brooks, M. E. Thompson and S. R. Forrest, High-efficiency yellow double-doped organic light-emitting devices based on phosphor-sensitized fluorescence, *Appl. Phys. Lett.*, 2001, **79**, 1045–1047.
- 7 C. Adachi, M. A. Baldo, S. R. Forrest, S. Lamansky, M. E. Thompson and R. C. Kwong, High-efficiency red electrophosphorescence devices, *Appl. Phys. Lett.*, 2001, **78**, 1622–1624.
- 8 S. Lamansky, P. Djurovich, D. Murphy, F. Abdel-Razzaq, R. Kwong, I. Tsyba, M. Bortz, B. Mui, R. Bau and M. E. Thompson, Synthesis and characterization of phosphorescent cyclometalated iridium complexes, *Inorg. Chem.*, 2001, **40**, 1704–1711.
- 9 A. B. Tamayo, B. D. Alleyne, P. I. Djurovich, S. Lamansky, I. Tsyba, N. N. Ho, R. Bau and M. E. Thompson, Synthesis and characterization of facial and meridional tris-cyclometalated iridium(III) complexes, *J. Am. Chem. Soc.*, 2003, **125**, 7377–7387.
- 10 R. J. Holmes, S. R. Forrest, Y.-J. Tung, R. C. Kwong, J. J. Brown, S. Garon and M. E. Thompson, Blue organic electrophosphorescence using exothermic host-guest energy transfer, *Appl. Phys. Lett.*, 2003, **82**, 2422–2424.
- 11 C. Wu, H.-F. Chen, K.-T. Wong and M. E. Thompson, Study of ion-paired iridium complexes (soft salts) and their application in organic light emitting diodes, *J. Am. Chem. Soc.*, 2010, **132**, 3133–3139.
- 12 B. Liu, F. Dang, Z. Feng, Z. Tian, J. Zhao, Y. Wu, X. Yang, G. Zhou, Z. Wu and W.-Y. Wong, Novel iridium(III) complexes bearing dimesitylboron groups with nearly 100% phosphorescent quantum yields for highly efficient organic light-emitting diodes, *J. Mater. Chem. C*, 2017, **5**, 7871–7883.
- 13 X. Yang, G. Zhou and W.-Y. Wong, Functionalization of phosphorescent emitters and their host materials by main-group elements for phosphorescent organic light-emitting devices, *Chem. Soc. Rev.*, 2015, **44**, 8484–8575.
- 14 Y. Im, S. Y. Byun, J. H. Kim, D. R. Lee, C. S. Oh, K. S. Yook and J. Y. Lee, Recent progress in high-efficiency blue-light-emitting materials for organic light-emitting diodes, *Adv. Funct. Mater.*, 2017, **27**, 1603007.
- 15 Z. Wu, N. Sun, L. Zhu, H. Sun, J. Wang, D. Yang, X. Qiao, J. Chen, S. M. Alshehri, T. Ahamad and D. Ma, Achieving extreme utilization of excitons by an efficient sandwich-type emissive layer architecture for reduced efficiency roll-off and improved operational stability in organic light-

emitting diodes, *ACS Appl. Mater. Interfaces*, 2016, **8**, 3150–3159.

16 J.-H. Lee, H. Shin, J.-M. Kim, K.-H. Kim and J.-J. Kim, Exciplex-forming co-host-based red phosphorescent organic light-emitting diodes with long operational stability and high efficiency, *ACS Appl. Mater. Interfaces*, 2017, **9**, 3277–3281.

17 K.-H. Kim, E. S. Ahn, J.-S. Huh, Y.-H. Kim and J.-J. Kim, Design of heteroleptic Ir complexes with horizontal emitting dipoles for highly efficient organic light-emitting diodes with an external quantum efficiency of 38%, *Chem. Mater.*, 2016, **28**, 7505–7510.

18 S.-Y. Kim, W.-I. Jeong, C. Mayr, Y.-S. Park, K.-H. Kim, J.-H. Lee, C.-K. Moon, W. Brüting and J.-J. Kim, Organic light-emitting diodes with 30% external quantum efficiency based on a horizontally oriented emitter, *Adv. Funct. Mater.*, 2013, **23**, 3896–3900.

19 S. Seo, S. Shitagaki, N. Ohsawa, H. Inoue, K. Suzuki, H. Nowatari and S. Yamazaki, Exciplex-triplet energy transfer: A new method to achieve extremely efficient organic light-emitting diode with external quantum efficiency over 30% and drive voltage below 3 V, *Jpn. J. Appl. Phys.*, 2014, **53**, 042102.

20 K.-H. Kim, S. Lee, C.-K. Moon, S.-Y. Kim, Y.-S. Park, J.-H. Lee and J.-J. Kim, Phosphorescent dye-based supramolecules for high-efficiency organic light-emitting diodes, *Nat. Commun.*, 2014, **5**, 4769.

21 X. Li, J. Zhang, Z. Zhao, L. Wang, H. Yang, Q. Chang and Z. Lu, Deep blue phosphorescent organic light-emitting diodes with CIEy value of 0.11 and external quantum efficiency up to 22.5%, *Adv. Mater.*, 2018, **30**, 1705005.

22 J.-H. Lee, S.-H. Cheng, S.-J. Yoo, H. Shin, J.-H. Chang, C.-I. Wu, K.-T. Wong and J.-J. Kim, An exciplex forming host for highly efficient blue organic light emitting diodes with low driving voltage, *Adv. Funct. Mater.*, 2015, **25**, 361–366.

23 H. Shin, J.-H. Lee, C.-K. Moon, J.-S. Huh, B. Sim and J.-J. Kim, Sky-blue phosphorescent OLEDs with 34.1% external quantum efficiency using a low refractive index electron transporting layer, *Adv. Mater.*, 2016, **28**, 4920–4925.

24 R. Zaen, K.-M. Park, K. H. Lee, J. Y. Lee and Y. Kang, Blue phosphorescent Ir(III) complexes achieved with over 30% external quantum efficiency, *Adv. Opt. Mater.*, 2019, **7**, 1901387.

25 Y. Zhang, J. Lee and S. R. Forrest, Tenfold increase in the lifetime of blue phosphorescent organic light-emitting diodes, *Nat. Commun.*, 2014, **5**, 5008.

26 X. Zhou, P. L. Burn and B. J. Powell, Bond fission and non-radiative decay in iridium(III) complexes, *Inorg. Chem.*, 2016, **55**, 5266–5273.

27 J. Lee, C. Jeong, T. Batagoda, C. Coburn, M. E. Thompson and S. R. Forrest, Hot excited state management for long-lived blue phosphorescent organic light-emitting diodes, *Nat. Commun.*, 2017, **8**, 15566.

28 D. Jacquemin and D. Escudero, The short device lifetimes of blue PhOLEDs: insights into the photostability of blue Ir(III) complexes, *Chem. Sci.*, 2017, **8**, 7844–7850.

29 S. Reineke, K. Walzer and K. Leo, Triplet-exciton quenching in organic phosphorescent light-emitting diodes with Ir-based emitters, *Phys. Rev. B: Condens. Matter Mater. Phys.*, 2007, **75**, 125328.

30 Y. Luo and H. Aziz, Correlation between triplet-triplet annihilation and electroluminescence efficiency in doped fluorescent organic light-emitting devices, *Adv. Funct. Mater.*, 2010, **20**, 1285–1293.

31 C. Murawski, K. Leo and M. C. Gather, Efficiency roll-off in organic light-emitting diodes, *Adv. Mater.*, 2013, **25**, 6801–6827.

32 S. Kim, H. J. Bae, S. Park, W. Kim, J. Kim, J. S. Kim, Y. Jung, S. Sul, S.-G. Ihn, C. Noh, S. Kim and Y. You, Degradation of blue-phosphorescent organic light-emitting devices involves exciton-induced generation of polaron pair within emitting layers, *Nat. Commun.*, 2018, **9**, 1211.

33 Y. You and S. Y. Park, Phosphorescent iridium(III) complexes: toward high phosphorescence quantum efficiency through ligand control, *Dalton Trans.*, 2009, 1267–1282.

34 W.-Y. Wong and C.-L. Ho, Functional metallophosphors for effective charge carrier injection/transport: new robust OLED materials with emerging applications, *J. Mater. Chem.*, 2009, **19**, 4457–4482.

35 Y. Chi and P.-T. Chou, Transition-metal phosphors with cyclometalating ligands: fundamentals and applications, *Chem. Soc. Rev.*, 2010, **39**, 638–655.

36 H. Fu, Y.-M. Cheng, P.-T. Chou and Y. Chi, Feeling blue? Blue phosphors for OLEDs, *Mater. Today*, 2011, **14**(10), 472–479.

37 K. S. Yook and J. Y. Lee, Organic materials for deep blue phosphorescent organic light-emitting diodes, *Adv. Mater.*, 2012, **24**, 3169–3190.

38 C.-L. Ho and W.-Y. Wong, Small-molecular blue phosphorescent dyes for organic light-emitting devices, *New J. Chem.*, 2013, **37**, 1665–1683.

39 R. Visbal and M. C. Gimeno, *N*-heterocyclic carbene metal complexes: photoluminescence and applications, *Chem. Soc. Rev.*, 2014, **43**, 3551–3574.

40 X. Yang, X. Xu and G. Zhou, Recent advances of the emitters for high performance deep-blue organic light-emitting diodes, *J. Mater. Chem. C*, 2015, **3**, 913–944.

41 I. Omae, Application of the five-membered ring blue light-emitting iridium products of cyclometalation reactions as OLEDs, *Coord. Chem. Rev.*, 2016, **310**, 154–169.

42 D. Ma, T. Tsuboi, Y. Qiu and L. Duan, Recent progress in ionic iridium(III) complexes for organic electronic devices, *Adv. Mater.*, 2017, **29**, 1603253.

43 C. E. Housecroft and E. C. Constable, Over the LEC rainbow: Colour and stability tuning of cyclometallated iridium(III) complexes in light-emitting electrochemical cells, *Coord. Chem. Rev.*, 2017, **350**, 155–177.

44 Y. Chi, T.-K. Chang, P. Ganesan and P. Rajakannu, Emissive bis-tridentate Ir(III) metal complexes: Tactics, photophysics and applications, *Coord. Chem. Rev.*, 2017, **346**, 91–100.

45 W. Song and J. Y. Lee, Degradation mechanism and lifetime improvement strategy for blue phosphorescent organic light-emitting diodes, *Adv. Opt. Mater.*, 2017, 1600901.

46 T.-Y. Li, J. Wu, Z.-G. Wu, Y.-X. Zheng, J.-L. Zuo and Y. Pan, Rational design of phosphorescent iridium(III) complexes for emission color tunability and their applications in OLEDs, *Coord. Chem. Rev.*, 2018, **374**, 55–92.

47 I. N. Mills, J. A. Porras and S. Bernhard, Judicious design of cationic, cyclometalated Ir(III) complexes for photochemical energy conversion and optoelectronics, *Acc. Chem. Res.*, 2018, **51**(2), 352–364.

48 H.-T. Maoa, G.-F. Li, G.-G. Shan, X.-L. Wang and Z.-M. Su, Recent progress in phosphorescent Ir(III) complexes for nondoped organic light-emitting diodes, *Coord. Chem. Rev.*, 2020, **413**, 213283.

49 R. Bai, X. Meng, X. Wang and L. He, Blue-emitting iridium(III) complexes for light-emitting electrochemical cells: Advances, challenges, and future prospects, *Adv. Funct. Mater.*, 2020, 1907169.

50 C. Zhang, R. Liu, D. Zhang and L. Duan, Progress on light-emitting electrochemical cells toward blue emission, high efficiency, and long lifetime, *Adv. Funct. Mater.*, 2020, 1907156.

51 A. Jablonski, Efficiency of anti-Stokes fluorescence in dyes, *Nature*, 1933, **131**, 839–840.

52 T. Hofbeck and H. Yersin, The triplet state of *fac*-Ir(ppy)<sub>3</sub>, *Inorg. Chem.*, 2010, **49**, 9290–9299.

53 P. J. Hay, Theoretical studies of the ground and excited electronic states in cyclometalated phenylpyridine Ir(III) complexes using density functional theory, *J. Phys. Chem. A*, 2002, **106**, 1634–1641.

54 A. V. Kukhta, I. N. Kukhta, S. A. Bagnich, S. M. Kazakov, V. A. Andreev, O. L. Neyra and E. Meza, Interactions of low-energy electrons with Ir(ppy)<sub>3</sub> in the gas phase, *Chem. Phys. Lett.*, 2007, **434**, 11–14.

55 A. R. G. Smith, P. L. Burn and B. J. Powell, Exact exchange and the density functional theory of metal-to-ligand charge-transfer in *fac*-Ir(ppy)<sub>3</sub>, *Org. Electron.*, 2016, **33**, 110–115.

56 E. Jansson, B. Minaev, S. Schrader and H. Ågren, Time-dependent density functional calculations of phosphorescence parameters for *fac*-tris(2-phenylpyridine) iridium, *Chem. Phys.*, 2007, **333**, 157–167.

57 B. Minaev, H. Ågren and F. De Angelis, Theoretical design of phosphorescence parameters for organic electroluminescence devices based on iridium complexes, *Chem. Phys.*, 2009, **358**, 245–257.

58 T. Matsushita, T. Asada and S. Koseki, Relativistic study on emission mechanism in tris (2-phenylpyridine) iridium, *J. Phys. Chem. C*, 2007, **111**, 6897–6903.

59 S. I. Bokarev, O. S. Bokareva and O. Kühn, Electronic excitation spectrum of the photosensitizer [Ir(ppy)<sub>2</sub>(bpy)]<sup>+</sup>, *J. Chem. Phys.*, 2012, **136**, 214305.

60 S. I. Bokarev, O. S. Bokareva and O. Kühn, A theoretical perspective on charge transfer in photocatalysis. The example of Ir-based systems, *Coord. Chem. Rev.*, 2015, **304**–**305**, 133–145.

61 S. Obara, M. Itabashi, F. Okuda, S. Tamaki, Y. Tanabe, Y. Ishii, K. Nozaki and M. Haga, Highly phosphorescent iridium complexes containing both tridentate bis (benzimidazolyl)-benzene or-pyridine and bidentate phenylpyridine: synthesis, photophysical properties, and theoretical study of Ir-bis(benzimidazolyl)benzene complex, *Inorg. Chem.*, 2006, **45**, 8907–8921.

62 K.-C. Tang, K. L. Liu and I.-C. Chen, Rapid intersystem crossing in highly phosphorescent iridium complexes, *Chem. Phys. Lett.*, 2004, **386**, 437–441.

63 H.-S. Duan, P.-T. Chou, C.-C. Hsu, J.-Y. Hung and Y. Chi, Photophysics of heteroleptic iridium(III) complexes of current interest; a closer look on relaxation dynamics, *Inorg. Chem.*, 2009, **48**, 6501–6508.

64 F. Spaenig, J.-H. Olivier, V. Prusakova, P. Retailleau, R. Ziessel and F. N. Castellano, Excited-state properties of heteroleptic iridium(III) complexes bearing aromatic hydrocarbons with extended cores, *Inorg. Chem.*, 2011, **50**(21), 10859–10871.

65 J. H. Klein, T. L. Sunderland, C. Kaufmann, M. Holzapfel, A. Schmiedel and C. Lambert, Stepwise versus pseudo-concerted two-electron-transfer in a triarylamine–iridium dipyrromethane diimide triad, *Phys. Chem. Chem. Phys.*, 2013, **15**, 16024–16030.

66 W. J. Finkenzeller and H. Yersin, Emission of Ir(ppy)<sub>3</sub>. Temperature dependence, decay dynamics, and magnetic field properties, *Chem. Phys. Lett.*, 2003, **377**, 299–305.

67 G. J. Hedley, A. Ruseckas and I. D. W. Samuel, Vibrational Energy Flow Controls Internal Conversion in a Transition Metal Complex, *J. Phys. Chem. A*, 2011, **114**, 8961–8968.

68 R. W. Harrigan and G. A. Crosby, Symmetry assignments of the lowest CT excited states of ruthenium(II) complexes via a proposed electronic coupling model, *J. Chem. Phys.*, 1973, **59**, 3468.

69 D. C. Baker and G. A. Crosby, Spectroscopic and magnetic evidence for multiple-state emission from tris(2,2'-bipyridine) ruthenium(II) sulfate, *Chem. Phys.*, 1974, **4**, 428–433.

70 H. Yersin and D. Donges, Low-lying electronic states and photophysical properties of organometallic Pd(II) and Pt (II) compounds. Modern research trends presented in detailed case studies, *Top. Curr. Chem.*, 2001, **214**, 81–186.

71 H. Wiedenhofer, S. Schuetzenmeier, A. v. Zelewsky and H. Yersin, Characterization of triplet sublevels by highly resolved vibrational satellite structures. Application to Pt (2-thpy)<sub>2</sub>, *J. Phys. Chem.*, 1995, **99**(36), 13385–13391.

72 Y. Koide, S. Takahashi and M. Vacha, Simultaneous two-photon excited fluorescence and one-photon excited phosphorescence from single molecules of an organometallic

complex  $\text{Ir}(\text{ppy})_3$ , *J. Am. Chem. Soc.*, 2006, **128**(34), 10990–10991.

73 E. Baranoff and B. F. E. Curchod, FIrpic: archetypal blue phosphorescent emitter for electroluminescence, *Dalton Trans.*, 2015, **44**, 8318–8329.

74 K. K.-W. Lo, C.-K. Chung, T. K.-M. Lee, K. H.-K. Tsang and N. Zhu, New luminescent cyclometalated iridium(III) diimine complexes as biological labeling reagents, *Inorg. Chem.*, 2003, **42**, 6886–6897.

75 H. Guo, M. L. Muro-Small, S. Ji, J. Zhao and F. N. Castellano, Naphthalimide Phosphorescence Finally Exposed in a Platinum(II) Diimine Complex, *Inorg. Chem.*, 2010, **49**, 6802–6804.

76 D. V. Kozlov, D. S. Tyson, C. Goze, R. Ziessel and F. N. Castellano, Room temperature phosphorescence from ruthenium(II) complexes bearing conjugated pyrenylethynylene subunits, *Inorg. Chem.*, 2004, **43**, 6083–6092.

77 A. F. Rausch, M. E. Thompson and H. Yersin, Blue light emitting  $\text{Ir}(\text{III})$  compounds for OLEDs-new insights into ancillary ligand effects on the emitting triplet state, *J. Phys. Chem. A*, 2009, **113**, 5927–5932.

78 T. Tsuboi, H. Murayama, S.-J. Yeh, M.-F. Wu and C.-T. Chen, Photoluminescence characteristics of blue phosphorescent  $\text{Ir}^{3+}$ -compounds FIrpic and FIrn4 doped in mCP and SimCP, *Opt. Mater.*, 2008, **31**, 366–371.

79 A. Endo, K. Suzuki, T. Yoshihara, S. Tobita, M. Yahiro and C. Adachi, Measurement of photoluminescence efficiency of  $\text{Ir}(\text{III})$  phenylpyridine derivatives in solution and solid-state films, *Chem. Phys. Lett.*, 2008, **460**, 155–157.

80 S.-C. Lo, C. P. Shipley, R. N. Bera, R. E. Harding, A. R. Cowley, P. L. Burn and I. D. W. Samuel, Blue phosphorescence from iridium(III) complexes at room temperature, *Chem. Mater.*, 2006, **18**, 5119–5129.

81 R. E. Harding, S.-C. Lo, P. L. Burn and I. D. W. Samuel, Non-radiative decay mechanisms in blue phosphorescent iridium(III) complexes, *Org. Electron.*, 2008, **9**, 377–384.

82 K. Huang and A. Rhys, Theory of light absorption and non-radiative transitions in  $F$ -centres, *Proc. R. Soc. London, Ser. A*, 1950, **204**, 406.

83 P. K. Mallick, G. D. Danzer, D. P. Strommen and J. R. Kincaid, Vibrational spectra and normal-coordinate analysis of tris(bipyridine)ruthenium(II), *J. Phys. Chem.*, 1988, **92**, 5628–5634.

84 T. Sajoto, P. I. Djurovich, A. B. Tamayo, J. Oxgaard, W. A. Goddard and M. E. Thompson, Temperature dependence of blue phosphorescent cyclometalated  $\text{Ir}(\text{III})$  complexes, *J. Am. Chem. Soc.*, 2009, **131**, 9813–9822.

85 R. D. Costa, F. Monti, G. Accorsi, A. Barbieri, H. J. Bolink, E. Ortí and N. Armaroli, Photophysical properties of charged cyclometalated  $\text{Ir}(\text{III})$  complexes: A joint theoretical and experimental study, *Inorg. Chem.*, 2011, **50**, 7229–7238.

86 L. Yang, F. Okuda, K. Kobayashi, K. Nozaki, Y. Tanabe, Y. Ishii and M. Haga, Syntheses and phosphorescent properties of blue emissive iridium complexes with tridentate pyrazolyl ligands, *Inorg. Chem.*, 2008, **47**, 7154–7165.

87 A. Juris, V. Balzani, F. Barigelli, S. Campagna, P. Belser and A. von Zelewsky, Ru(II) polypyridine complexes: photophysics, photochemistry, electrochemistry, and chemiluminescence, *Coord. Chem. Rev.*, 1988, **84**, 85–277.

88 J. H. Seo, Y. K. Kim and Y. Ha, Efficient blue-green organic light-emitting diodes based on heteroleptic tris-cyclometalated iridium(III) complexes, *Thin Solid Films*, 2009, **517**, 1807–1810.

89 R. Ragni, E. A. Plummer, K. Brunner, J. W. Hofstraat, F. Babudri, G. M. Farinola, F. Naso and L. De Cola, Blue emitting iridium complexes: synthesis, photophysics and phosphorescent devices, *J. Mater. Chem.*, 2006, **16**, 1161–1170.

90 X. Li, B. Minaev, H. Ågren and H. Tian, Theoretical study of phosphorescence of iridium complexes with fluorine-substituted phenylpyridine ligands, *Eur. J. Inorg. Chem.*, 2011, 2517–2524.

91 F. De Angelis, S. Fantacci, N. Evans, C. Klein, S. M. Zakeeruddin, J.-E. Moser, K. Kalyanasundaram, H. J. Bolink, M. Grätzel and M. K. Nazeeruddin, Controlling phosphorescence color and quantum yields in cationic iridium complexes: a combined experimental and theoretical study, *Inorg. Chem.*, 2007, **46**, 5989–6001.

92 T. Karatsu, M. Takahashi, S. Yagai and A. Kitamura, Photophysical properties of substituted homoleptic and heteroleptic phenylimidazolinato  $\text{Ir}(\text{III})$  complexes as a blue phosphorescent material, *Inorg. Chem.*, 2013, **52**, 12338–12350.

93 H. Cho, J. Lee, J.-I. Lee, N. S. Cho, J. H. Park, J. Y. Lee and Y. Kang, Phenylimidazole-based homoleptic iridium(III) compounds for blue phosphorescent organic light-emitting diodes with high efficiency and long lifetime, *Org. Electron.*, 2016, **34**, 91–96.

94 Y. Kwon, S. H. Han, S. Yu, J. Y. Lee and K. M. Lee, Functionalized phenylimidazole-based facial-homoleptic iridium(III) complexes and their excellent performance in blue phosphorescent organic light-emitting diodes, *J. Mater. Chem. C*, 2018, **6**, 4565–4572.

95 K. Tamao, M. Uchida, T. Izumizawa, K. Furukawa and S. Yamaguchi, Silole derivatives as efficient electron transporting materials, *J. Am. Chem. Soc.*, 1996, **118**, 11974–11975.

96 A. R. G. Smith, M. J. Riley, P. L. Burn, I. R. Gentle, S.-C. Lo and B. J. Powell, Effects of fluorination on iridium(III) complex phosphorescence: magnetic circular dichroism and relativistic time-dependent density functional theory, *Inorg. Chem.*, 2012, **51**, 2821–2831.

97 S.-C. Lo, R. N. Bera, R. E. Harding, P. L. Burn and I. D. W. Samuel, Solution-processible phosphorescent blue dendrimers based on biphenyl-dendrons and *fac*-tris(phenyltriazolyl)iridium(III) cores, *Adv. Funct. Mater.*, 2008, **18**, 3080–3090.

98 S.-C. Lo, R. E. Harding, E. Brightman, P. L. Burn and I. D. W. Samuel, The development of phenylethylene dendrons for blue phosphorescent emitters, *J. Mater. Chem.*, 2009, **19**, 3213–3227.

99 S.-C. Lo, R. E. Harding, C. P. Shipley, S. G. Stevenson, P. L. Burn and I. D. W. Samuel, High-triplet-energy dendrons: enhancing the luminescence of deep blue phosphorescent iridium(III) complexes, *J. Am. Chem. Soc.*, 2009, **131**, 16681–16688.

100 Y. Wang, Y. Lu, B. Gao, S. Wang, J. Ding, L. Wang, X. Jing and F. Wang, Self-host blue-emitting iridium dendrimer containing bipolar dendrons for nondoped electrophosphorescent devices with superior high-brightness performance, *ACS Appl. Mater. Interfaces*, 2016, **8**, 29600–29607.

101 Y. Wang, Y. Lu, B. Gao, S. Wang, J. Ding, L. Wang, X. Jing and F. Wang, Single molecular tuning of the charge balance in blue-emitting iridium dendrimers for efficient nondoped solution-processed phosphorescent OLEDs, *Chem. Commun.*, 2016, **52**, 11508–11511.

102 Y. Wang, S. Wang, J. Ding, L. Wang, X. Jing and F. Wang, Dendron engineering in self-host blue iridium dendrimers towards low-voltage-driving and power-efficient nondoped electrophosphorescent devices, *Chem. Commun.*, 2017, **53**, 180–183.

103 J. Wang, J. Peng, C. Yao, R. Liu, W. Yao, C. Zhang, M. He and C. Jiang, Self-host blue-emitting iridium dendrimer for solution-processed non-doped phosphorescent organic light-emitting diodes with flat efficiency roll-off and less phase segregation, *Org. Electron.*, 2017, **45**, 49–56.

104 G. Zhang, F. Hermerschmidt, A. Pramanik, D. Schollmeyer, M. Baumgarten, P. Sarkar, E. J. W. List-Kratochvil and K. Müllen, Bulky, dendronized iridium complexes and their photoluminescence, *J. Mater. Chem. C*, 2019, **7**, 15252–15258.

105 C. Adachi, R. C. Kwong, P. Djurovich, V. Adamovich, M. A. Baldo, M. E. Thompson and S. R. Forrest, Endothermic energy transfer: A mechanism for generating very efficient high-energy phosphorescent emission in organic materials, *Appl. Phys. Lett.*, 2001, **79**, 2082–2084.

106 J. Li, P. I. Djurovich, B. D. Alleyne, M. Yousufuddin, N. N. Ho, J. C. Thomas, J. C. Peters, R. Bau and M. E. Thompson, Synthetic control of excited-state properties in cyclometalated Ir(III) complexes using ancillary ligands, *Inorg. Chem.*, 2005, **44**, 1713–1727.

107 I. Avilov, P. Minoofar, J. Cornil and L. De Cola, Influence of substituents on the energy and nature of the lowest excited states of heteroleptic phosphorescent Ir(III) complexes: A joint theoretical and experimental study, *J. Am. Chem. Soc.*, 2007, **129**, 8247–8258.

108 E. Orselli, G. S. Kottas, A. E. Konradsson, P. Coppo, R. Fröhlich, L. De Cola, A. van Dijken, M. Büchel and H. Börner, Blue-emitting iridium complexes with substituted 1,2,4-triazole ligands: Synthesis, photophysics, and devices, *Inorg. Chem.*, 2007, **46**, 11082–11093.

109 E. Orselli, R. Q. Albuquerque, P. M. Fransen, R. Fröhlich, H. M. Janssenc and L. De Cola, 1,2,3-Triazolyl-pyridine derivatives as chelating ligands for blue iridium(III) complexes. Photophysics and electroluminescent devices, *J. Mater. Chem.*, 2008, **18**, 4579–4590.

110 Y. Feng, X. Zhuang, D. Zhu, Y. Liu and M. R. Bryce, Rational design and characterization of heteroleptic phosphorescent iridium(III) complexes for highly efficient deep-blue OLEDs, *J. Mater. Chem. C*, 2016, **4**, 10246–10252.

111 Y.-J. Cho, S.-Y. Kim, J.-H. Kim, D. W. Crandell, M.-H. Baik, J. Lee, C. H. Kim, H.-J. Son, W.-S. Han and S. O. Kang, Important role of ancillary ligand in the emission behaviours of blue-emitting heteroleptic Ir(III) complexes, *J. Mater. Chem. C*, 2017, **5**, 4480–4487.

112 V. Sivasubramaniam, F. Brodkorb, S. Hanning, H. P. Loebel, V. van Elsbergen, H. Boerner, U. Scherf and M. Kreyenschmidt, Fluorine cleavage of the light blue heteroleptic triplet emitter FIrpic, *J. Fluor. Chem.*, 2009, **130**, 640–649.

113 B. Liu, M. A. Jabed, J. Guo, W. Xu, S. L. Brown, A. Ugrinov, E. K. Hobbie, S. Kilina, A. Qin and W. Sun, Neutral cyclometalated iridium(III) complexes bearing substituted N-heterocyclic carbene (NHC) ligands for high-performance yellow OLED application, *Inorg. Chem.*, 2019, **58**, 14377–14388.

114 J.-H. Zhao, Y.-X. Hu, H.-Y. Lu, Y.-L. Lü and X. Li, Progress on benzimidazole-based iridium(III) complexes for application in phosphorescent OLEDs, *Org. Electron.*, 2017, **41**, 56–72.

115 G. Sarada, B. Sim, W. Cho, J. Yoon, Y.-S. Gal, J.-J. Kim and S.-H. Jin, New sky-blue and bluish-green emitting Ir(III) complexes containing an azoline ancillary ligand for highly efficient PhOLEDs, *Dyes Pigm.*, 2016, **131**, 60–68.

116 N. M. Shavaleev, R. Scopelliti, M. Grätzel, M. K. Nazeeruddin, A. Pertegás, C. Roldán-Carmona, D. Tordera and H. J. Bolink, Pulsed-current versus constant-voltage light-emitting electrochemical cells with trifluoromethyl-substituted cationic iridium(III) complexes, *J. Mater. Chem. C*, 2013, **1**, 2241–2248.

117 D. Cortés-Arriagada, L. Sanhueza, I. González, P. Dreyse and A. Toro-Labbé, About the electronic and photo-physical properties of iridium(III)-pyrazino[2,3-f][1,10]-phenanthroline based complexes for use in electroluminescent devices, *Phys. Chem. Chem. Phys.*, 2016, **18**, 726–734.

118 P. Tao, Y. Zhang, J. Wang, L. Wei, H. Li, X. Li, Q. Zhao, X. Zhang, S. Liu, H. Wang and W. Huang, Highly efficient blue phosphorescent iridium(III) complexes with various ancillary ligands for partially solution-processed organic light-emitting diodes, *J. Mater. Chem. C*, 2017, **5**, 9306–9314.

119 Y. Miao, P. Tao, L. Gao, X. Li, L. Wei, S. Liu, H. Wang, B. Xu and Q. Zhao, Highly efficient chlorine functionalized blue iridium(III) phosphors for blue and white phosphorescent organic light-emitting diodes with the external quantum efficiency exceeding 20%, *J. Mater. Chem. C*, 2018, **6**, 6656–6665.

120 J.-P. Zhang, Y. Wang, J.-B. Ma, L. Jin, F.-T. Liu and F.-Q. Bai, Density functional theory investigation on

iridium(III) complexes for efficient blue electrophosphorescence, *RSC Adv.*, 2018, **8**, 19437–19448.

121 A. K. Pal, S. Krotkus, M. Fontani, C. F. R. Mackenzie, D. B. Cordes, A. M. Z. Slawin, I. D. W. Samuel and E. Zysman-Colman, High-efficiency deep-blue-emitting organic light-emitting diodes based on iridium (III) carbene complexes, *Adv. Mater.*, 2018, **30**, 1804231.

122 A. F. Henwood and E. Zysman-Colman, Lessons learned in tuning the optoelectronic properties of phosphorescent iridium(III) complexes, *Chem. Commun.*, 2017, **53**, 807–826.

123 A. K. Pal, A. F. Henwood, D. B. Cordes, A. M. Z. Slawin, I. D. W. Samuel and E. Zysman-Colman, Blue-to-green emitting neutral Ir(III) complexes bearing pentafluorosulfanyl groups: a combined experimental and theoretical study, *Inorg. Chem.*, 2017, **56**, 7533–7544.

124 C. D. Ertl, J. Cerdá, J. M. Junquera-Hernández, A. Pertegás, H. J. Bolink, E. C. Constable, M. Neuburger, E. Ortí and C. E. Housecroft, Colour tuning by the ring roundabout:  $[\text{Ir}(\text{C}^{\text{N}})^2(\text{N}^{\text{N}})]^+$  emitters with sulfonyl-substituted cyclometallating ligands, *RSC Adv.*, 2015, **5**, 42815–42827.

125 J.-H. Kim, S.-Y. Kim, S. Jang, S. Yi, D. W. Cho, H.-J. Son and S. O. Kang, Blue phosphorescence with high quantum efficiency engaging the trifluoromethylsulfonyl group to iridium phenylpyridine complexes, *Inorg. Chem.*, 2019, **58**, 16112–16125.

126 H. Benjamin, M. A. Fox, A. S. Batsanov, H. A. Al-Attar, C. Li, Z. Ren, A. P. Monkman and M. R. Bryce, Pyridylpyrazole N<sup>N</sup>N ligands combined with sulfonyl-functionalised cyclometalating ligands for blue-emitting iridium(III) complexes and solution-processable PhOLEDs, *Dalton Trans.*, 2017, **46**, 10996–11007.

127 R. J. Holmes and S. R. Forrest, Saturated deep blue organic electrophosphorescence using a fluorine-free emitter, *Appl. Phys. Lett.*, 2005, **87**, 243507.

128 S. Díez-González, N. Marion and S. P. Nolan, *N*-heterocyclic carbenes in late transition metal catalysis, *Chem. Rev.*, 2009, **109**, 3612–3676.

129 M. N. Hopkinson, C. Richter, M. Schedler and F. Glorius, An overview of *N*-heterocyclic carbenes, *Nature*, 2014, **510**, 485–496.

130 C.-H. Chien, S. Fujita, S. Yamato, T. Hara, T. Yamagata, M. Watanabe and K. Mashima, Stepwise and one-pot syntheses of Ir(III) complexes with imidazolium-based carbene ligands, *Dalton Trans.*, 2008, 916–923.

131 T. Sajoto, P. I. Djurovich, A. Tamayo, M. Yousufuddin, R. Bau and M. E. Thompson, Blue and near-UV phosphorescence from iridium complexes with cyclometalated pyrazolyl or *N*-heterocyclic carbene ligands, *Inorg. Chem.*, 2005, **44**, 7992–8003.

132 S. Haneder, E. Da Como, J. Feldmann, J. M. Lupton, C. Lennartz, P. Erk, E. Fuchs, O. Molt, I. Münster, C. Schildknecht and G. Wagenblast, Controlling the radiative rate of deep-blue electrophosphorescent organo-metallic complexes by singlet-triplet gap engineering, *Adv. Mater.*, 2008, **20**, 3325–3330.

133 C.-F. Chang, Y.-M. Cheng, Y. Chi, Y.-C. Chiu, C.-C. Lin, G.-H. Lee, P.-T. Chou, C.-C. Chen, C.-H. Chang and C.-C. Wu, Highly efficient blue-emitting iridium(III) carbene complexes and phosphorescent OLEDs, *Angew. Chem., Int. Ed.*, 2008, **47**, 4542–4545.

134 Y. Liu, X. Sun, G. Gahungu, X. Qu, Y. Wang and Z. Wu, DFT/TDDFT investigation on the electronic structures and photophysical properties of phosphorescent Ir(III) complexes with conjugated/non-conjugated carbene ligands, *J. Mater. Chem. C*, 2013, **1**, 3700–3709.

135 H. Sasabe, J. Takamatsu, T. Motoyama, S. Watanabe, G. Wagenblast, N. Langer, O. Molt, E. Fuchs, C. Lennartz and J. Kido, High-efficiency blue and white organic light-emitting devices incorporating a blue iridium carbene complex, *Adv. Mater.*, 2010, **22**, 5003–5007.

136 K. Tsuchiya, S. Yagai, A. Kitamura, T. Karatsu, K. Endo, J. Mizukami, S. Akiyama and M. Yabe, Synthesis and photophysical properties of substituted tris(phenylbenzimidazolinato) IrIII carbene complexes as a blue phosphorescent material, *Eur. J. Inorg. Chem.*, 2010, 926–933.

137 N. Darmawan, C.-H. Yang, M. Mauro, M. Raynal, S. Heun, J. Pan, H. Buchholz, P. Braunstein and L. De Cola, Efficient near-UV emitters based on cationic bis-pincer iridium(III) carbene complexes, *Inorg. Chem.*, 2013, **52**, 10756–10765.

138 T.-Y. Li, X. Liang, L. Zhou, C. Wu, S. Zhang, X. Liu, G.-Z. Lu, L.-S. Xue, Y.-X. Zheng and J.-L. Zuo, *N*-Heterocyclic carbenes: Versatile second cyclometalated ligands for neutral iridium(III) heteroleptic complexes, *Inorg. Chem.*, 2015, **54**, 161–173.

139 Z. Chen, S. Suramitr, N. Zhu, C.-L. Ho, S. Hannongbua, S. Chen and W.-Y. Wong, Tetrafluorinated phenylpyridine based heteroleptic iridium(III) complexes for efficient sky blue phosphorescent organic light-emitting diodes, *J. Mater. Chem. C*, 2020, **8**, 2551–2557.

140 J. Lee, H.-F. Chen, T. Batagoda, C. Coburn, P. I. Djurovich, M. E. Thompson and S. R. Forrest, Deep blue phosphorescent organic light-emitting diodes with very high brightness and efficiency, *Nat. Mater.*, 2015, **15**, 92–99.

141 X. Zhou and B. J. Powell, Nonradiative decay and stability of *N*-heterocyclic carbene iridium(III) complexes, *Inorg. Chem.*, 2018, **57**, 8881–8889.

142 Z. Chen, L. Wang, S. Su, X. Zheng, N. Zhu, C.-L. Ho, S. Chen and W.-Y. Wong, Cyclometalated iridium(III) carbene phosphors for highly efficient blue organic light-emitting diodes, *ACS Appl. Mater. Interfaces*, 2017, **9**, 40497–40502.

143 B.-S. Yun, J.-H. Kim, S.-Y. Kim, H.-J. Son, D. W. Cho and S. O. Kang, Photophysical properties of structural isomers of homoleptic Ir-complexes derived from xlenyl-substituted *N*-heterocyclic carbene ligands, *Phys. Chem. Chem. Phys.*, 2019, **21**, 7155–7164.

144 Y.-J. Cho, S.-Y. Kim, J.-H. Kim, J. Lee, D. W. Cho, S. Yi, H.-J. Son, W.-S. Han and S. O. Kang, Probing photo-

physical properties of isomeric *N*-heterocyclic carbene Ir(III) complexes and their applications to deep-blue phosphorescent organic light-emitting diodes, *J. Mater. Chem. C*, 2017, **5**, 1651–1659.

145 H. Na, L. M. Canada, Z. Wen, J. I. Wu and T. S. Teets, Mixed-carbene cyclometalated iridium complexes with saturated blue luminescence, *Chem. Sci.*, 2019, **10**, 6254–6260.

146 Y.-C. Chiu, J.-Y. Hung, Y. Chi, C.-C. Chen, C.-H. Chang, C.-C. Wu, Y.-M. Cheng, Y.-C. Yu, G.-H. Lee and P.-T. Chou, En Route to High External Quantum Efficiency (~12%), Organic True-Blue-Light-Emitting Diodes Employing Novel Design of Iridium(III) Phosphors, *Adv. Mater.*, 2009, **21**, 2221–2225.

147 N. P. Ayala, C. M. Flynn Jr., L. Sacksteder, J. N. Demas and B. A. DeGraff, Synthesis, luminescence, and excited-state complexes of the tris(1,10-phenanthroline)- and bis(teripyridine)iridium(III) cations, *J. Am. Chem. Soc.*, 1990, **112**, 3837–3844.

148 J.-P. Collin, I. M. Dixon, J.-P. Sauvage, J. A. G. Williams, F. Barigelli and L. Flamigni, Synthesis and photophysical properties of iridium(III) bisterpyridine and its homologues: a family of complexes with a long-lived excited state, *J. Am. Chem. Soc.*, 1999, **121**, 5009–5016.

149 A. J. Wilkinson, H. Puschmann, J. A. K. Howard, C. E. Foster and J. A. G. Williams, Luminescent complexes of iridium(III) containing N<sub>3</sub>C<sub>6</sub>N-coordinating terdentate ligands, *Inorg. Chem.*, 2006, **45**, 8685–8699.

150 V. L. Whittle and J. A. G. Williams, A new class of iridium complexes suitable for stepwise incorporation into linear assemblies: Synthesis, electrochemistry, and luminescence, *Inorg. Chem.*, 2008, **47**, 6596–6607.

151 V. L. Whittle and J. A. G. Williams, Cyclometallated, bis-terdentate iridium complexes as linearly expandable cores for the construction of multimetallic assemblies, *Dalton Trans.*, 2009, 3929–3940.

152 A. J. Wilkinson, A. E. Goeta, C. E. Foster and J. A. G. Williams, Synthesis and luminescence of a charge-neutral, cyclometalated iridium(III) complex containing N<sub>3</sub>C<sub>6</sub>N- and C<sub>6</sub>N<sub>3</sub>- coordinating terdentate ligands, *Inorg. Chem.*, 2004, **43**, 6513–6515.

153 T. Yutaka, S. Obara, S. Ogawa, K. Nozaki, N. Ikeda, T. Ohno, Y. Ishii, K. Sakai and M. Haga, Syntheses and properties of emissive iridium(III) complexes with tridentate benzimidazole derivatives, *Inorg. Chem.*, 2005, **44**, 4737–4746.

154 J. A. G. Williams, A. J. Wilkinson and V. L. Whittle, Light-emitting iridium complexes with tridentate ligands, *Dalton Trans.*, 2008, 2081–2099.

155 C.-Y. Kuei, W.-L. Tsai, B. Tong, M. Jiao, W.-K. Lee, Y. Chi, C.-C. Wu, S.-H. Liu, G.-H. Lee and P.-T. Chou, Bis-tridentate Ir(III) complexes with nearly unitary RGB phosphorescence and organic light-emitting diodes with external quantum efficiency exceeding 31%, *Adv. Mater.*, 2016, **28**, 2795–2800.

156 H.-H. Kuo, Y.-T. Chen, L. R. Devereux, C.-C. Wu, M. A. Fox, C.-Y. Kuei, Y. Chi and G.-H. Lee, Bis-tridentate Ir(III) metal phosphors for efficient deep-blue organic light-emitting diodes, *Adv. Mater.*, 2017, **29**, 1702464.

157 H.-H. Kuo, Z. Zhu, C.-S. Lee, Y.-K. Chen, S.-H. Liu, P.-T. Chou, A. K.-Y. Jen and Y. Chi, Bis-tridentate iridium(III) phosphors with very high photostability and fabrication of blue-emitting OLEDs, *Adv. Sci.*, 2018, **5**, 1800846.

158 Y.-K. Chen, H.-H. Kuo, D. Luo, Y.-N. Lai, W.-C. Li, C.-H. Chang, D. Escudero, A. K.-Y. Jen, L.-Y. Hsu and Y. Chi, Phenyl-and pyrazolyl-functionalized pyrimidine: versatile chromophore of bis-tridentate Ir(III) phosphors for organic light-emitting diodes, *Chem. Mater.*, 2019, **31**, 6453–6464.

159 H.-H. Kuo, L.-Y. Hsu, J.-Y. Tso, W.-Y. Hung, S.-H. Liu, P.-T. Chou, K.-T. Wong, Z.-L. Zhu, C.-S. Lee, A. K.-Y. Jen and Y. Chi, Blue-emitting bis-tridentate Ir(III) phosphors: OLED performances vs. substituent effects, *J. Mater. Chem. C*, 2018, **6**, 10486–10496.

160 V. Adamovich, P.-L. Boudeault, M. A. Esteruelas, D. Gómez-Bautista, A. M. López, E. Oñate and J.-Y. Tasi, Preparation via a NHC dimer complex, photophysical properties, and device performance of heteroleptic bis (tridentate) iridium(III) emitters, *Organometallics*, 2019, **38**, 2738–2747.

161 J.-L. Liao, P. Rajakannu, S.-H. Liu, G.-H. Lee, P.-T. Chou, A. K.-Y. Jen and Y. Chi, Iridium(III) complexes bearing tridentate chromophoric chelate: phosphorescence fine-tuned by phosphine and hydride ancillary, *Inorg. Chem.*, 2018, **57**, 8287–8298.

162 L.-Y. Hsu, Q. Liang, Z. Wang, H.-H. Kuo, W.-S. Tai, S.-J. Su, X. Zhou, Y. Yuan and Y. Chi, Bis-tridentate Ir(III) Phosphors bearing two fused five-six-membered metallacycles: A strategy to improved photostability of blue Emitters, *Chem. – Eur. J.*, 2019, **25**, 15375–15386.

163 V. L. Whittle and J. A. G. Williams, A New Class of Iridium Complexes Suitable for Stepwise Incorporation into Linear Assemblies: Synthesis, Electrochemistry, and Luminescence, *Inorg. Chem.*, 2008, **47**, 6596–6607.

164 A. Tsuboyama, T. Takiguchi, S. Okada, M. Osawa, M. Hoshino and K. Ueno, A novel dinuclear cyclometalated iridium complex bridged with 1,4-bis[pyridine-2-yl]benzene: its structure and photophysical properties, *Dalton Trans.*, 2004, 1115–1116.

165 F. Neve, A. Crispini, S. Serroni, F. Loiseau and S. Campagna, Novel dinuclear luminescent compounds based on iridium(III) cyclometalated chromophores and containing bridging ligands with ester-linked chelating sites, *Inorg. Chem.*, 2001, **40**, 1093–1101.

166 L. Donato, C. E. McCusker, F. N. Castellano and E. Zysman-Colman, Mono- and dinuclear cationic iridium(III) complexes bearing a 2,5-dipyridylpyrazine (2,5-dpp) ligand, *Inorg. Chem.*, 2013, **52**, 8495–8504.

167 J. Fernández-Cestau, N. Giménez, E. Lalinde, P. Montaño, M. T. Moreno and S. Sánchez, Synthesis, characterization, and properties of doubly alkynyl bridging dinuclear cyclo-

metallated iridium(III) complexes, *Organometallics*, 2015, **34**, 1766–1778.

168 D. G. Congrave, Y.-T. Hsu, A. S. Batsanov, A. Beeby and M. R. Bryce, Synthesis, Diastereomer separation, and optoelectronic and structural properties of dinuclear cyclometalated iridium(III) complexes with bridging diarylhydrazide ligands, *Organometallics*, 2017, **36**, 981–993.

169 G. Li, D. G. Congrave, D. Zhu, Z. Su and M. R. Bryce, Recent advances in luminescent dinuclear iridium(III) complexes and their application in organic electroluminescent devices, *Polyhedron*, 2018, **140**, 146–157.

170 G. Li, D. Zhu, X. Wang, Z. Su and M. R. Bryce, Dinuclear metal complexes: multifunctional properties and applications, *Chem. Soc. Rev.*, 2020, **49**, 765–838.

171 D. G. Congrave, Y.-T. Hsu, A. S. Batsanov, A. Beeby and M. R. Bryce, Sky-blue emitting bridged diiridium complexes: beneficial effects of intramolecular  $\pi$ – $\pi$  stacking, *Dalton Trans.*, 2018, **47**, 2086–2098.

172 D. G. Congrave, A. S. Batsanov and M. R. Bryce, Highly luminescent 2-phenylpyridine-free diiridium complexes with bulky 1,2-diarylimidazole cyclometalating ligands, *Dalton Trans.*, 2018, **47**, 16524–16533.

173 J.-L. Liao, P. Rajakannu, P. Gnanasekaran, S.-R. Tasi, C.-H. Lin, S.-H. Liu, C.-H. Chang, G.-H. Lee, P.-T. Chou, Z.-N. Chen and Y. Chi, Luminescent diiridium complexes with bridging pyrazolates: Characterization and fabrication of OLEDs using vacuum thermal deposition, *Adv. Opt. Mater.*, 2018, **6**, 1800083.

174 S. Yi, J.-H. Kim, Y.-J. Cho, J. Lee, T.-S. Choi, D. W. Cho, C. Pac, W.-S. Han, H.-J. Son and S. O. Kang, Stable blue phosphorescence iridium(III) cyclometalated complexes prompted by intramolecular hydrogen bond in ancillary ligand, *Inorg. Chem.*, 2016, **55**, 3324–3331.

175 X. Wang, H. Yang, Y. Wen, L. Wang, J. Li and J. Zhang, Comprehension of the effect of a hydroxyl group in ancillary ligand on phosphorescent property for heteroleptic Ir(III) complexes: a computational study using quantitative prediction, *Inorg. Chem.*, 2017, **56**, 8986–8995.